Dead Volume Effects in Passive Regeneration: Experimental and Numerical Characterization

by

Yifeng Liu

BEng., Northwestern Polytechnical University, 2011

A Thesis Submitted in Partial Fulfillment of the Requirements for the Degree of

MASTER OF APPLIED SCIENCE

in the

Department of Mechanical Engineering

Supervisory Committee

Dead Volume Effects in Passive Regeneration: Experimental and Numerical Characterization

by

Yifeng Liu
BEng., Northwestern Polytechnical University, 2011

Supervisory Committee

Dr. Andrew Rowe Department of Mechanical Engineering
Supervisor

Dr. Rustom Bhiladvala Department of Mechanical Engineering
Departmental Member

Abstract

Supervisory Committee

Dr. Andrew Rowe Department of Mechanical Engineering

Supervisor

Dr. Rustom Bhiladvala Department of Mechanical Engineering

Departmental Member

The regenerator is the key component in magnetic cycles for refrigeration and heat pumping. It works as temporal thermal energy storage and separates two thermal reservoirs. Regenerators are typically made up of porous structures which may create complex flow pathways for the heat transfer fluid through the regenerator. The periodically reversing flow allows the thermal energy exchange with the packing material in the regenerators. The performance of such thermal devices depends greatly on the geometry of the porous structure, material properties as well as operating conditions.

This thesis is a study about the thermo-hydraulic properties of passive regenerators under oscillating flow conditions. The first part of the thesis presents a passive regenerator testing apparatus used to measure temperature distribution and pressure drop for various types of regenerators. Three kinds of loose spheres packed regenerator beds are characterized, and the regenerator effectiveness is evaluated. In the second part of the thesis, a numerical model is developed for the predictions of pressure drop and temperature field, and the theoretical findings are applied to experimentally obtained data to interpret regenerator performance. The dead volume is investigated quantitatively and considered to affect the regenerator performance adversely.

Table of Contents

List of Figures

List of Tables

Nomenclature

Acronyms

AMR	Active magnetic refrigerator
MCE	Magnetocaloric effect
NTU	Number of transfer unit

Symbols

A	Area [m^2]
A_c	Cross-sectional area of regenerator [m^2]
A_f	Flow area of regenerator [m^2]
A_s	Solid are of regenerator [m^2]
A_w	Wetted surface area of regenerator matrix [m^2]
B_i	Biot number [-]
C_E	Ergun constant [-]
c_f	Specific heat capacity of fluid [J/kgK]
c_s	Specific heat capacity of solid [J/kgK]
D	Regenerator diameter [m]
D_i	Inner diameter of tube [m]
D_o	Outer diameter of tube [m]

D_{os} Outer diameter of insulation foam [m]

D_p Particle diameter [m]

e Regenerator matrix porosity [-]

f_0 Constant in effective conductivity of regenerator [-]

F_o Fourier number [-]

H_{act_cb} Actual enthalpy change during cold blow [J]

h_f Thermal convection coefficient [W/Km^2]

h_{eff} Effective thermal convection coefficient [W/Km^2]

H_{max_cb} Theoretical maximum enthalpy change during cold blow [J]

K Permeability of regenerator matrix

k_{air} Thermal conduction coefficient of air [W/Km]

$k_{dynamic}$ Effective dynamic thermal conduction coefficient of regenerator [W/Km]

k_f Thermal conduction coefficient of fluid [W/Km]

k_{ins} Thermal conduction coefficient of insulation [W/Km]

k_s Thermal conduction coefficient of solid [W/Km]

k_{static} Effective static thermal conduction coefficient of regenerator [W/Km]

k_{tube} Thermal conduction coefficient of tube [W/Km]

L_{dv} Dead volume length [m]

L_{reg} Regenerator length [m]

m_{dv_f} Mass of fluid in dead volume [kg]

m_f	Mass of fluid in regenerator [kg]
m_s	Mass of solid in regenerator [kg]
$\dot{m}$	Fluid mass flow rate [kg/s]
N_u	Nusselt number [-]
p	Pressure [Pa]
P_e	Peclet number [-]
P_r	Prandtl number [-]
$\dot{Q}_{cond\_f}$	Rate of heat conduction in fluid [W]
$\dot{Q}_{cond\_s}$	Rate of heat conduction in solid [W]
$\dot{Q}_{conv\_f}$	Rate of heat convection from solid to fluid [W]
$\dot{Q}_{conv\_s}$	Rate of heat convection from fluid to solid [W]
$\dot{Q}_{dv\_flux}$	Rate of fluid enthalpy flux in dead volume [W]
$\dot{Q}_{dv\_cond\_f}$	Rate of heat conduction in dead volume fluid [W]
$\dot{Q}_{dv\_conv\_f}$	Rate of heat convection from the ambient to fluid in dead volume[W]
$\dot{Q}_{flux}$	Rate of fluid enthalpy flux [W]
R_{air}	Thermal resistance of air [K/W]
R_{dv}	Total thermal resistance between dead volume and the ambient [K/W]
R_{ep}	Reynolds number based on particle diameter [-]
R_{eh}	Reynolds number based on hydraulic diameter [-]
R_{ins}	Thermal resistance of insulation [K/W]
R_{tube}	Thermal resistance of tube [K/W]

T	Temperature [K]
t	Non-dimensionalized time [-]
$\tilde{t}$	Time [s]
T_{amb}	Temperature of the ambient [K]
T_{CHEX}	Cold heat exchanger temperature [K]
T_f	Temperature of the fluid [K]
T_{HHEX}	Hot heat exchanger temperature [K]
T_s	Temperature of the solid [K]
u_D	Darcy velocity [m/s]
$\dot{U}_f$	Energy change rate of fluid [W]
$\dot{U}_s$	Energy changer rate of solid [W]
$\dot{U}_{dv\_f}$	Energy change rate of fluid in dead volume [W]
$\dot{W}_{vis}$	Viscous dissipation rate [W]
x	Non-dimensionalized spatial parameter [-]
$\tilde{x}$	Spatial parameter [m]

Greek

α_0	Constant in effective conductivity of regenerator [-]
β	Degradation factor for internal temperature gradient [-]
γ	Linear factor for static conduction coefficient [-]
ε_C	Regenerator cold end effectiveness [-]

ε_H	Regenerator hot end effectiveness [-]
ε_{TOT}	Total regenerator effectiveness [-]
σ	Linear factor for dynamic conduction coefficient [-]
λ	Linear factor for convection coefficient [-]
τ_b	Time period of a single blow [s]
ρ_f	Fluid density [kg/m^3]
ρ_s	Solid density [kg/m^3]
Λ	Effectiveness imbalance between regenerator hot and cold ends [-]
Φ	Utilization [-]
$\dot{\Phi}$	Transient utilization [/s]

Common Subscript

amb	Ambient
c	Cold end
dv	Dead volume
f	Fluid
s	Solid

Acknowledgement

Completing this master’s program has been such a great and unforgettable experience for me. Thank my supervisor, Andrew, for always being patient and supportive. Thank the Cryofuels group, for all the knowledge and joy in and out of the lab. And thank my father and mother, I could not have been here without you.

Introduction

1.1 Overview

Increasing energy consumption and the associated environmental concerns of modern society present challenges to traditional technologies, but also bring opportunities to potentially more efficient and cleaner processes. Taking the U.S as an example, during the year 2014, 3.2 quadrillion BTU of energy delivered by electricity, including residential and commercial sectors, is used by heating and cooling applications. And it will be increased to 3.8 quadrillion BTU by the year of 2035, according to the data released by U.S. Energy Information Administration [1]. Hence, there is a need for more efficient heating and cooling technologies.

Conventional heat pumps near room temperature use vapour-compression cycles to produce either heating or cooling effect. This technology has been developed and refined for decades, and has proven its robustness and applicability in both industrial and domestic fields. In refrigeration cycles with vapour-compression, popular chemical refrigerant may possess global warming potential [2]. Like any other technology, vapour-compression processes are susceptible to irreversibilities which lower the device operating efficiency. Given the maturity of conventional vapor compression refrigerators, alternative technologies are being investigated to meet new performance demands. Among those emerging technologies, magnetic heat pumps are receiving increased attention.

In magnetic refrigeration, the cooling effect is produced through the magnetization and demagnetization of an environmentally neutral solid refrigerant [3]. Furthermore, a magnetic cycle does not require compressors or throttles, avoiding some of the

irreversibilities seen in conventional cycles. There is the potential for increased device operating efficiency over conventional refrigeration systems [4].

1.2 Magnetic Cycles

Like traditional thermal devices based on simple-compressible substances, cycles can be created using simple-magnetic materials; these are materials which have a magnetic work mode. One can define magnetic cycles that use heat to produce work, or use work input to pump heat as in a refrigerator or heat pump. The phrase *heat pump* can describe a device that provides useful cooling or a device that provides heat, as the cycles can be the same, but the desired effect is different. Magnetic refrigeration is based on the phenomenon called magnetocaloric effect (MCE). It can be described as the isothermal entropy change or the adiabatic temperature change due to the introduction of a magnetic field. A substance with MCE is able to achieve a useful temperature change when adiabatically subjected to a change in applied magnetic field. In conventional materials, a positive temperature change is measured with a positive field change; however, a negative temperature change is seen in some materials. The magnitude of this temperature change depends on the material type, absolute temperature and strength of the applied magnetic field. For some materials, the temperature increase is significant enough to form the basis of a thermal cycle. This effect can be either almost fully reversible or presenting hysteresis, depending on the characteristics of the material. In the reversible case, removing the magnetic field will make the material revert back to the original temperature. An active magnetic refrigerator (AMR) uses the magnetic refrigerant itself as an active regenerator in the refrigeration cycle. The idea was developed by Barclay and Steyert in 1982 to greatly improve performance [5], when compared to previous magnetic refrigeration design consisting of passive regenerators and heat exchangers.

An active magnetic regenerator refrigerator (AMRR) is a cooling device based on an active magnetic regenerator cycle. The principle of AMRR operation can be explained approximately as a system with a magnetic Brayton cycle, comprised of two adiabatic processes and two isofield processes, as summarized below.

(1) The active magnetic regenerator is adiabatically magnetized, resulting in an isentropic temperature rise through the bed due to the MCE;
(2) Heat transfer fluid is blown through the bed from the cold end to the hot end, the heat collected is rejected to the hot sink via a heat exchanger;
(3) The regenerator is adiabatically demagnetized, leading to an isentropic temperature drop through the bed;
(4) Heat transfer fluid is blown through the bed from the hot end to the cold end, refrigerating a thermal load on the cold end.

This basic cycle has been demonstrated experimentally and numerically to create useful heat pumping; however, to achieve a magnetic refrigerator comparable to conventional gas compression refrigerators, further work is needed on novel magnetic material development [6]–[8], new magnetic field source arrangement [9], [10] effective regenerator configuration [11], [12], optimal operating parameters determination [13], [14] and thermal efficiency optimization [15].

1.3 Passive Regenerator Testing

Due to the expense and complexity of AMR devices, the use of passive devices is common during the early stages of regenerator development. Passive regenerator testing involves characterization of regenerator geometries in absence of magnetic fields, including pressure drop and heat transfer studies, to find optimal operating conditions and regenerator geometry. In passive testing, there is no investment in magnets and the regenerator can be fabricated with more conventional materials, which do not have MCE, leading to lower research cost and shorter experimental cycles [16].

A practical consideration in the design of AMR systems is the thermal connection between the regenerators and the heat exchangers that are interacting with the loads and thermal reservoirs. The heat transfer fluid physically carries the energy absorbed at the cold heat exchanger into the AMR. The AMR then pumps the heat to higher temperature where is advected by the heat transfer fluid to the hot heat exchanger. Ideally, the fluid exiting the regenerators should make thermal contact with the external heat exchangers so as to maximize heat transfer rates. Because fluid is oscillating in some areas of the apparatus with a mean displacement of zero, the fluid may not be displaced far enough to reach any other location in the regenerator or in the external fluid system. This is minimized in the regenerator matrix by using small porosities and sufficient displaced fluid volume; however, to ensure pressure drop is not too high, larger flow areas are used externally which can lead to volumes where fluid is confined on average. These fluid volumes decrease the thermal link between the heat exchangers and the regenerator and lead to decreased performance. For this reason, the flow volumes between the external heat exchangers and the regenerator are known as *dead volume*, as shown in Figure 1-1.

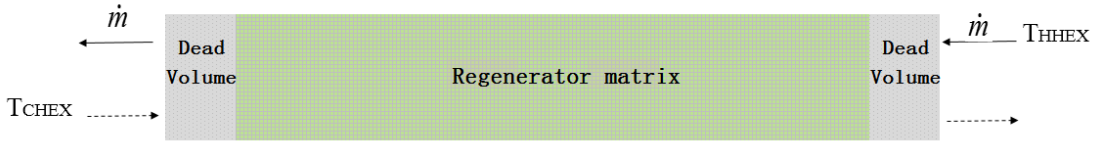

Figure 0-1 Regenerator and dead volume domains demonstration, dead volume is on each side of the regenerator domain.

Dead volume impacts have been mentioned by some authors as reasons for poor performance in AMR systems [17], [18]. Dead volume occurs in AMR systems as oscillatory or bi-directional flow takes place. Some research shows that dead volume negatively affects the cooling power generated by AMR, and the reduction of the performance gets larger according to the increase in dead volume [19]. Hence, the potential loss due to dead volume should be as small as possible in AMR designs. One

common method is using valves to make the flow uni-directional beyond the AMR, and keeping the valve system as close as possible with regard to the AMR and the heat exchangers to avoid or minimize the dead volume. In an AMR, the displaced fluid volume is often similar to the volume of solid material in the matrix depending on the thermal mass of the fluid and the solid. To date, no study has quantified the relationship between displaced fluid volume, dead volume and effectiveness.

1.4 Objectives

Many experimental devices and numerical models developed for magnetic refrigeration research use beds of packed spheres or parallel plates [20]–[22], but neither of them has been proved ideal because of either large viscous losses or inadequate heat transfer. A vast amount of literature exists on the optimization of oscillating-flow regenerators using gases [23]. There is relatively little work examining regenerators using liquids. In addition, experimental studies of regenerators often use unidirectional transient flow which can lead to different heat transfer properties than oscillating flow conditions using water [24].

This work aims at establishing a clear experimental and numerical methodology to quantify viscous losses and heat transfer effectiveness for oscillating flow through a porous matrix. Results focus on various packed beds of spheres over a range of operating conditions common to AMR cycles. The objective is to provide guidance for regenerator optimization and to understand how dead volume impacts the effectiveness of the regenerator process. The research described in this thesis is comprised of the following activities.

(1) Experimental characterization including apparatus modifications, test procedure development, and data acquisition handing.

(2) Creation of a numerical model to simulate regenerator performance.

(3) Validation of numerical simulations using experimental results.

(4) Interpretation of regenerator performance due to external dead volume effects.

The work will be described in the following chapters beginning with a description of the experimental apparatus, the material used in the experiments, and the test condition. The numerical model is described in Chapter 3 along with the transport expressions, boundary conditions and simulation parameters. Chapter 4 and 5 present the results of the experiments and simulations. This is followed by a critical discussion of results and key findings. Chapter 7 summarizes the findings and suggests areas for further research.

Experimental Method

This chapter describes the passive regenerator testing apparatus. It includes descriptions of the experimental setup, regenerator building method, regenerator types, experimental operations, and data processing.

2.1 Experimental Apparatus

A passive regenerator testing apparatus is designed to measure the thermal-hydraulic properties of passive regenerators under oscillating flow using liquid heat transfer fluid. The key parameters determining performance are pressure drop across the regenerator and the transient temperature distribution. Figure 2-1 shows the schematic of the current device.

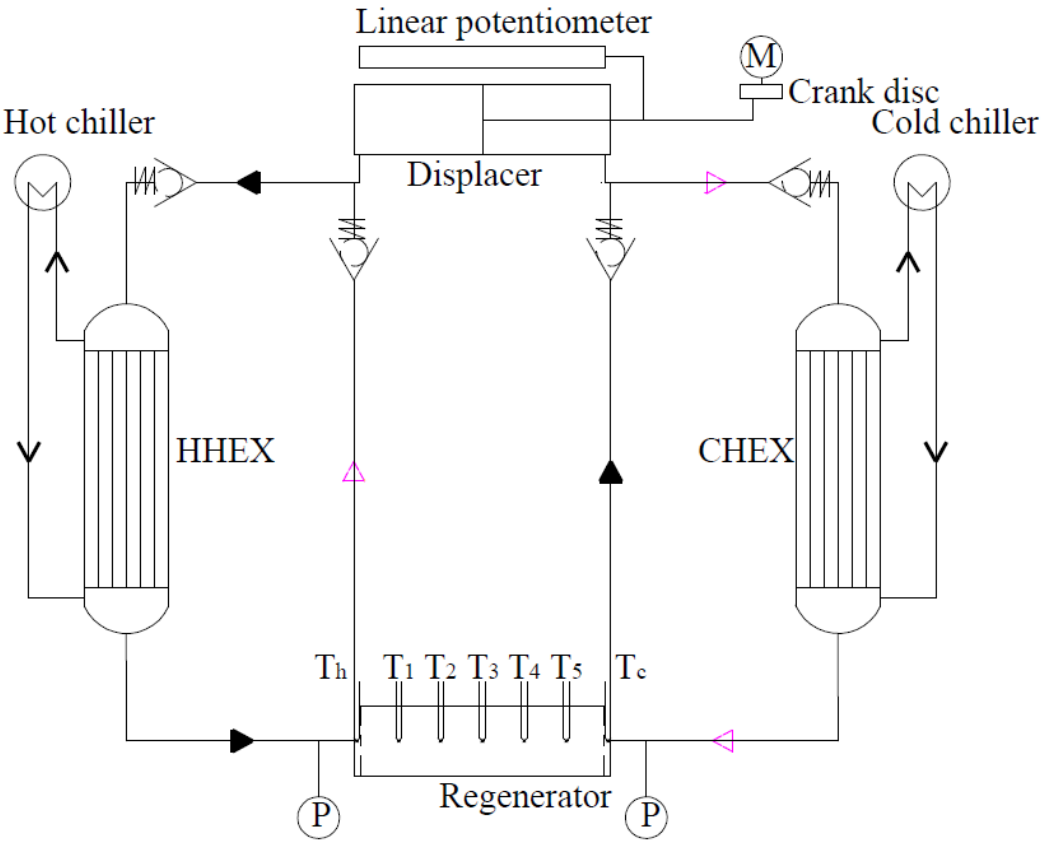

Figure 0-1 A schematic of current passive regenerator test apparatus demonstrates all units and the flow directions.

As shown in Figure 2-1, two chillers (Julabo FCW2500T and Thermo NESLab RTE740) are used as the thermal reserviors for the cold and hot sides of the regenerator respectively.

Two custom shell-and-tube heat exchangers thermally couple the regenerator heat transfer fluid to the chillers. The heat exchanger surface is a bundle of aluminum tubes creating channels through which the regenerator heat transfer flows. A plexi glass tube with inner diameter of 38 mm is used as the shell which confines the chiller fluid flow.

Four check valves work collaboratively to keep the flow unidirectional when it is travelling through the heat exchangers. The check valves help reduce the dead volume in the system; however, there is still a certain amount of dead volume existing in the system due to the tube fittings. The impact of dead volume will be further discussed in the results.

An electric motor drives a displacer (Bimba 043-DXDE and 122.5 DXDE) via a crank mechanism which creates oscillating flow in the system. The stroke of the displacer is controlled by changing the position of the rod connection point on the crank disk. A linear potentiometer (Omega® LP802-75) is coupled with the displacer to measure the instantaneous displacer position and determine fluid flow rate.

Seven type E thermocouples (Omega® EMQSS-020G-6) are located along the regenerator to collect the temperature distribution and variation during the experiments, with probes reaching the center of the regenerator cylinder, as we can see in Figure 2-2. The diameter of the thermocouple probe is smaller than the diameter of the spheres, so as to minimize the change in local flow geometry due to the presence of the thermocouples. Taking one end of the regenerator shell as reference, the thermocouples are positioned at 0 mm, 15 mm, 32.5 mm, 50 mm, 60 mm, 85 mm and 100 mm. Two pressure transducers (Omega® PX613) measure the instantaneous pressure simultaneously at the ends of the regenerator. Another four thermocouples are used to

measure the inlet and outlet temperatures of the heat exchangers. A thermocouple module (National Instruments 9213) and a module for pressure transducers and linear potentiometer (National Instruments 9205) are used to acquire all the data from the sensors. Both modules are mounted on a compact DAQ carrier (National Instruments cDAQ 9174).

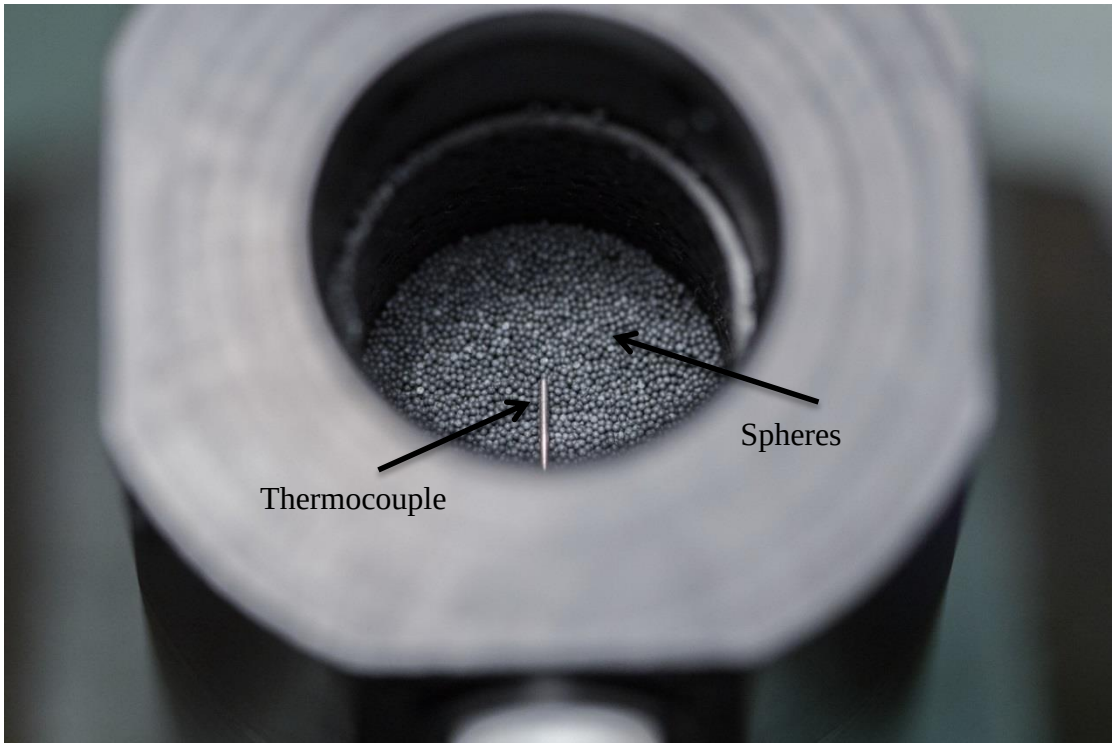

Figure 0-2 One of the thermocouples lies inside the regenerator housing, it’s covered by spherical particles as well.

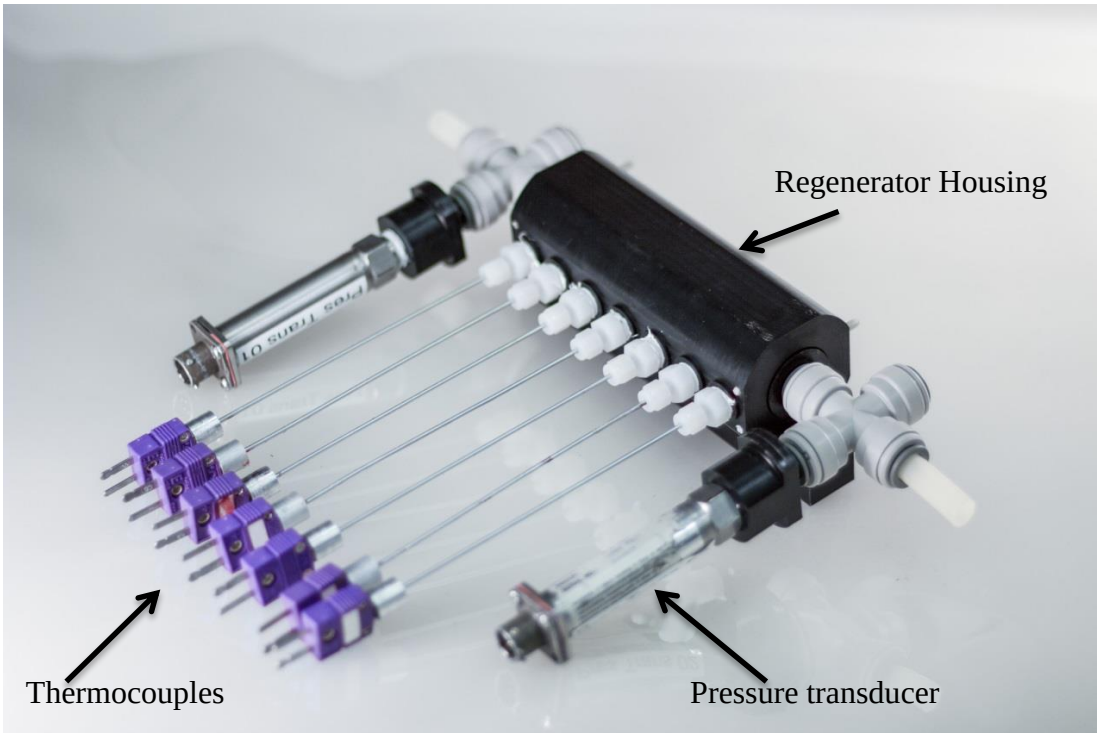

Figure 0-3 Assembly of the regenerator, thermocouples and pressure transducers, is ready to be linked to displacer and heat exchangers.

In the work described here, the regenerator beds are made up of loose packed spherical particle beds. The spheres are held in position by fine wire mesh adjacent to the end of the matrix. The mesh screens separate the regenerator matrix from the external flow system via two end-connectors as shown in Figure 2-4. The connectors are push-to-connect tees; a pressure transducer is connected to one of the ports and the other two ports act as inlet and outlet connections for the fluid flow. The direction of the flow is constrained by check valves so that fluid leaving the regenerator is directed through the external heat exchanger prior to re-entering the bed. The end thermocouple is inserted through both the regenerator housing and the end connector, located beyond the mesh screen and 1 mm away from the regenerator matrix.

2.2 Assembly Procedure

To assemble a regenerator bed, a connector is attached to one end with wire mesh. A certain quantity of particles are then used to fill a fraction of the housing up the point

where a thermocouple probe enters the cavity through the housing wall. The probe is located so that the tip is at the center of the housing. Then, another layer of particles is added up to next probe location where the thermocouple is placed. This procecure is repeated. After the regenerator housing is filled with particles, it is closed with an end connector. Careful packing and positioning is needed to make sure that every thermocouple takes the measurement at the correct location.

Figure 0-4 End connector of the regenerator consists of one push-to-connect tee, a mesh screen and an o ring.

Once the regenerator housing is packed and closed with the end connectors, the shell can then be connected to the fluid flow and heat exchange system. The whole device is charged with fluid by making use of a charging machine, which mainly consists of a motor, a pump, a fluid reservoir and tubing. In order to get the air out from the device, the charging process is repeated several times with the flow direction being changed. In addition, the device is pressurized to 60 psi to push the air out from the device through two bleeding valves.

2.3 Matrix Types

Three different materials are tested: stainless steel, lead and gadolinium. The specific heat capacities for each material are shown in Figure 2-5 where it can be seen that both lead and stainless steel have little variation over the temperature range of interest [25], [26].

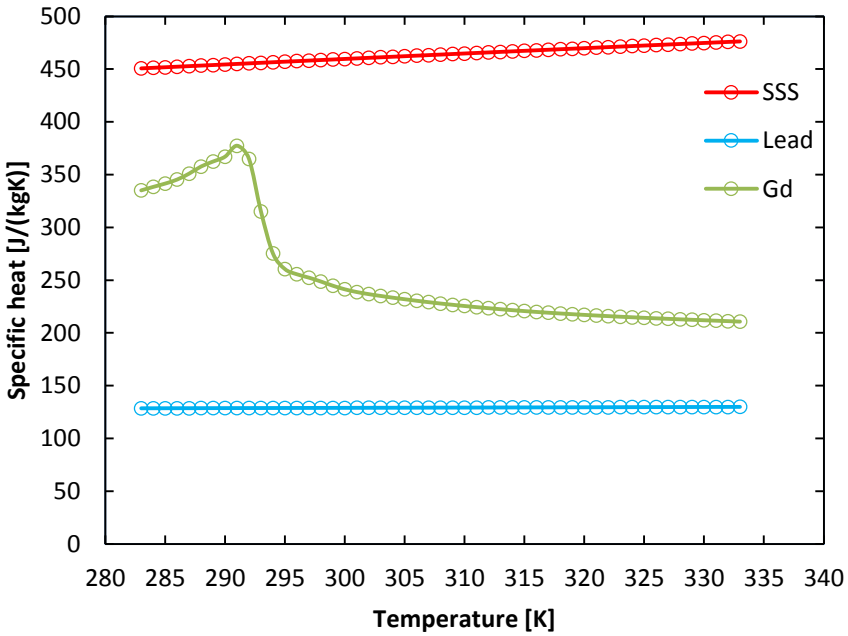

Figure 0-5 Specific heat capacities of stainless steel, lead and gadolinium are presented as a function of temperature

Gadolinium undergoes a transition from ferromagnetic to paramagnetic as the temperature increases past the Curie point of approximately 293 K. As a result, the specific heat capacity is a strong function of temperature in this region. The thermal properties of each material are summarized in Table 2-1.

Table 0-1 Regenerator materials properties

	Stainless steel [25]	Lead [25]	Gadolinium [26]
Density [kg/m^3]	7900	11030	7900
Conductivity [W/(m•K)]	16	35	11
Specific heat [J/(kg•K)]	500	130	variable

Table 0-2 Experimental parameters for the three types of beds

	Stainless steel	Lead	Gadolinium
Sphere diameter [mm]	1	0.5	0.5
Regenerator length [mm]	100	100	100
Regenerator mass [g]	0.166	0.233	0.166
Porosity [-]	0.36	0.36	0.36

The porosity of each regenerators is 36%, which is estimated based on the dimensions of the housing and the volumes of material.

2.3.1 Utilization

An important parameter governing regenerator performance is the ratio of thermal capacity of the fluid displaced to the thermal mass of the matrix. This quantity if called the *utilization* and is numerically determined in Equation (2.1). The numerator is the thermal mass of fluid displaced in the regenerator and is determined by the specific heat, c_f, and the displaced mass, m_{dis}. The denominator is the total mass of solid matrix, m_s, and the specific heat of the solid material, c_s.

$$\Phi = \frac{m_{dis} c_f}{m_s c_s} \tag{2.1}$$

In order to cover a utilization range of 0.3 to 1.1, the specific heat of the matrix and the mass of material are used to determine the displaced fluid volume and the size of the displacer. Because of the temperature dependence of specific heat for gadolinium, a reference utilization is calculated using specific heat at the transition temperature of 293 K. A 0.75 inch diameter displacer (nominal bore size) (Bimba® 043-DXDE) is used for the tests on lead spheres and a 1.25 inch diameter displacer (Bimba® 122.5 DXDE) is used for the tests on stainless steel spheres and gadolinium spheres.

In this work, the heat transfer fluid is distilled water. Using the specific heat of water, the utilizations and corresponding displaced fluid volumes for each of the three different material are listed Table 2-3. Discrete values are determined by the diameter of a displacer and the set increments in the connecting rod position on the crank-arm.

Table 0-3 Utilization ranges for each bed during tests.

Regenerator bed	Displaced fluid volume [cm^3]	Utilization
Stainless steel	6.95, 10.43, 13.9, 17.37, 20.85	0.37, 0.56, 0.74, 0.93, 1.11
Lead	2.53, 3.80, 5.06, 6.33, 7.59	0.36, 0.53, 0.71, 0.89,1.07
Gadolinium	6.95, 10.43, 13.9, 17.37	0.50, 0.75, 100, 1.24

2.3.2 Estimation of Dead Volume Size

Even though check valves are used to minimize dead volume in the device, a certain amount of dead volume still exists and affects the experiments. The impact of dead volume is studied experimentally and numerically. To do so it requires quantifying the size of the dead volume in the experimental configuration. The inner diameter and length of the tubing between the end thermocouple and the heat exchanger are measured to calculate the volume.

To gain a better understanding of the dead volume impact, a set of experiments are performed where the dead volume is varied. Dead volume is varied by changing the volume between the heat exchangers and the regenerator.

2.4 Testing Procedure

An experiment begins by using the two chillers to set the temperature span across the regenerator. For the experiments described here, the fluid exiting the hot heat exchanger is set to be 50 C and the cold heat exchanger is set to 10 C. Imperfect insulation of the tubing between the heat exchangers and regenerator results in a change in temperature of the fluid. The temperature change is a function of utilization and frequency so some adjustments to chiller set-points are made as need to ensure the operating span across the regenerator is nearly the same for all tests (+/- 0.1K). Results are normalized by span so small deviations are acceptable. Nominally, the temperature span is constant so that the average solid and thermal properties are the same for each test.

The voltage input for the displacer drive motor is set to give the desired operating frequency. This frequency is calculated and displayed in Labview based on the measured pressures and displacer movements; the frequency has an uncertainty of +/- 0.005Hz. A linear potentiometer is excited with a constant input voltage of 5 volts giving an output which is consequently 0 to 5. The stroke of the linear potentiometer is 76 mm; thus the sensitivity is 15 mm/volt.

Once the displacer is started, the system reaches cyclic steady state, in approximately 10 minutes. Steady-state is determined based on the change in the temperature distributions in the regenerator. When the maximum and minimum temperature measurements at each location are constant within +/- 0.2K, steady-state is assumed. Once the system gets to a steady state, the temperature variations of the two thermocouples at the ends of the regenerator are checked. If the inlet temperature are significantly different than the desired settings, the chiller temperatures are changed to eliminate the difference. This is repeated until the desired operating span is achieved at which point data collection begins for a number of cycles.

A different sampling rate is used for each operating frequency so that the same angular discretization of the waveform is obtained. A cycle is discretized by 300 evenly spaced samples, such that if the operating frequency is 1 Hz then the sampling rate is 300 Hz. The range of frequencies is 0.25 Hz to 1.5 Hz with an increment of 0.25 Hz. Three cycles of data are used for regenerator effectiveness and pressure drop calculations. Under periodic steady state the temperature and pressure variations are repeatable from one cycle to another.

2.5 Data processing

A common metric used to quantify the thermal performance of passive regenerators is the *effectiveness*. The effectiveness is the ratio between the actual enthalpy change through the regenerator and the equivalent maximum theoretical enthalpy change in an

ideal regenerator during a single blow [27], [28]. This definition includes the pumping energy due to viscous dissipation. As we can consider the enthalpy change of the fluid as it flows from the cold side to the hot side, or hot to cold, there are two effectiveness values that can be defined – the hot blow effectiveness and the cold blow effectiveness [29]. A *hot blow* is the portion of a cycle when the fluid is flowing from the hot side to the cold side, a *cold blow* is the other half of the cycle.

Taking the cold blow effectiveness as example, we assume fluid is entering the cold face of the regenerator at constant temperature, and, as the blow progresses, the fluid exiting the hot end progressively decreases in temperature. This process is shown schematically in Figure 2-6.

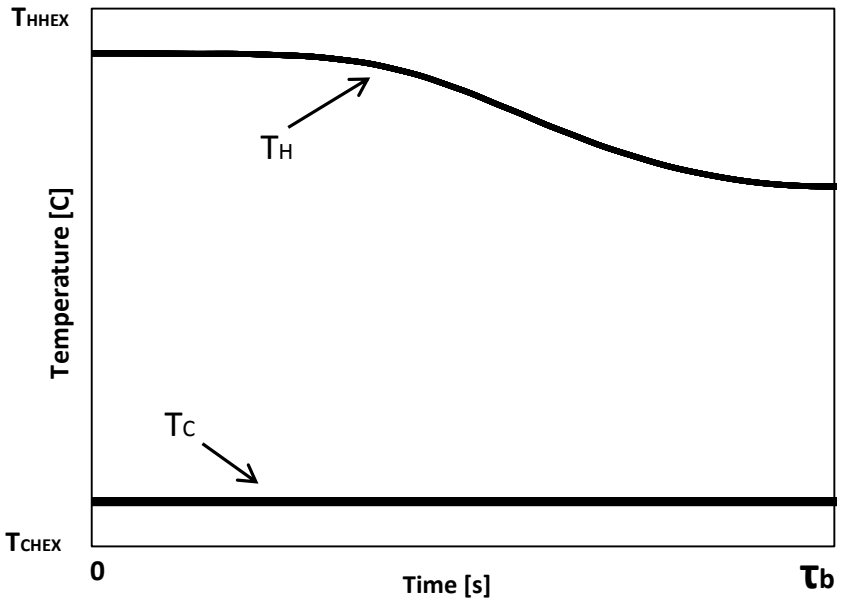

Figure 0-6 Temperature profiles of the regenerator hot side and cold side during a cold blow, the temperature on the hot side drops as the blow propagates through the regenerator.

The cold blow effectiveness of the regenerator is calculated as below.

$$\varepsilon_{CB} = \frac{H_{act,CB}}{H_{\max,CB}} \tag{2.2}$$

where H_{act_CB} is the actual enthalpy change through the regenerator during a cold blow and H_{max_CB} is the equivalent maximum theoretical enthalpy change in an ideal regenerator.

$$H_{act,CB} = \int_0^{\tau_b} \dot{m}(\tilde{t}) \cdot (h(T_H, p_H) - h(T_C, p_C)) d\tilde{t} \tag{2.3}$$

Assuming the fluid is incompressible and specific heat is constant, the above becomes

$$H_{act,CB} = \int_0^{\tau_b} \dot{m}(\tilde{t}) \cdot [c_f ((T_H(\tilde{t}) - T_C(\tilde{t})) + \frac{1}{\rho_f}(p_H(\tilde{t}) - p_C(\tilde{t})]d\tilde{t} \tag{2.4}$$

$$H_{act,CB} = \int_0^{\tau_b} \dot{m}(\tilde{t}) \cdot [c_f ((T_H(\tilde{t}) - T_C(\tilde{t}))]d\tilde{t} - W_{vis} \tag{2.5}$$

where

$$W_{vis} = -\int_0^{\tau_b} \frac{\dot{m}(\tilde{t})}{\rho_f}(p_H(\tilde{t}) - p_C(\tilde{t}))d\tilde{t} \tag{2.6}$$

Assuming flow is positive, the above expression results in a positive quantity for pump work. The ideal regenerator would have no pressure drop, infinite heat transfer rate, and infinite thermal mass such that the maximum enthalpy change of the fluid would be,

$$H_{\max\_cb} = \int_0^{\tau_b} \dot{m}(\tilde{t}) \cdot c_f (T_{HHEX} - T_{CHEX}) d\tilde{t} \tag{2.7}$$

Hence, the cold blow effectiveness is

$$\varepsilon_{CB} = \frac{\int_0^{\tau_b} \dot{m}(\tilde{t}) \cdot [c_f ((T_H(\tilde{t}) - T_C(\tilde{t}))]d\tilde{t} - W_{vis}}{m_d c_f (T_{HHEX} - T_{CHEX})} \tag{2.8}$$

A similar derivation can made for the blow period where fluid is flowing from the hot side to the cold side. As with the previous derivation, the direction of fluid flow is assumed to be the positive direction so that the mass flow rate is positive during the blow. The results for the hot to cold flow period then appears as follows.

$$\varepsilon_{HB} = \frac{\int_{\tau_b}^{2\tau_b} \dot{m}(\tilde{t}) \cdot [c_f ((T_C(\tilde{t}) - T_H(\tilde{t}))]d\tilde{t} - W_{vis}}{m_d c_f (T_{CHEX} - T_{HHEX})} \tag{2.9}$$

Or, multiplying top and bottom by -1,

$$\varepsilon_{HB} = \frac{\int_{\tau_b}^{2\tau_b} \dot{m}(\tilde{t}) \cdot [c_f((T_H(\tilde{t}) - T_C(\tilde{t}))] d\tilde{t} + W_{vis}}{m_d c_f (T_{HHEX} - T_{CHEX})} \tag{2.10}$$

The expressions for hot and cold blow effectiveness show that because the viscous work term is always positive, for the same temperature change, the hot blow effectiveness can be larger than the cold blow.

Normally, the pumping work is small compared with the internal energy of the fluid, resulting in a negligible contribution to the effectiveness calculation. When pumping work is negligible the regenerator effectiveness expressions are simplified to:

$$\varepsilon_{CB} = \frac{\int_{0}^{\tau_b} \dot{m}(\tilde{t}) \cdot [c_f((T_H(\tilde{t}) - T_C(\tilde{t}))] d\tilde{t}}{m_d c_f (T_{HHEX} - T_{CHEX})} \tag{2.11}$$

$$\varepsilon_{HB} = \frac{\int_{\tau_b}^{2\tau_b} \dot{m}(\tilde{t}) \cdot [c_f((T_H(\tilde{t}) - T_C(\tilde{t}))] d\tilde{t}}{m_d c_f (T_{HHEX} - T_{CHEX})} \tag{2.12}$$

It is possible that ε_H is different from ε_C. A parameter to quantify the imbalance between these two terms is defined in Equation 2.13. This effectiveness imbalance can be either greater or smaller than unity, resulting from various factors including axial heat conduction and temperature-dependent material properties.

$$\Lambda = \frac{\varepsilon_{CB}}{\varepsilon_{HB}} \tag{2.13}$$

The average pressure drop is extracted from the experimental data using Equation 2.14.

$$\overline{\Delta p} = \frac{1}{2\tau_b} (\left| \int_0^{\tau_b} (p_H(\tilde{t}) - p_C(\tilde{t})) d\tilde{t} \right| + \left| \int_{\tau_b}^{2\tau_b} (p_H(\tilde{t}) - p_C(\tilde{t})) d\tilde{t} \right|) \tag{2.14}$$

The experimental aspects including the testing apparatus, regenerator matrix type, testing procedures and data processing have been explained. In next chapter the numerical model will be derived and described.

Model Development

This chapter describes numerical models predicting the pressure drop and temperature field through passive regenerator beds. The model determines the spatial and temporal temperatures of the fluid and solid at cyclic steady-state conditions. Physical phenomena such as dispersion, diffusion, convection and viscous dissipation are included. In addition, the effects of transvers heat leak and dead volumes on each end of the regenerator are considered. A detailed description follows starting with the one-dimensional momentum equation for porous media.

3.1 Pressure Model

A general Navier-Stokes equation for incompressible flow is as following [30].

$$\rho_f \left(\frac{\partial \boldsymbol{v}}{\partial \tilde{t}} + \boldsymbol{v} \cdot \nabla \boldsymbol{v}\right) = -\nabla p + \mu \nabla^2 \boldsymbol{v} + \boldsymbol{f} \tag{3.1}$$

In this volume averaged equation, ρ_f is the density of the fluid, $\boldsymbol{v}$ is the velocity vector, p is the pressure, μ is the dynamic viscosity of the fluid, f is the field of external force and ∇ is the gradient operator.

A phenomenological approach for porous media includes a Darcy term and Ergun inertial term into the equation [30], [31],

$$\rho_f \left(\frac{\partial \boldsymbol{v}}{\partial \tilde{t}} + \boldsymbol{v} \cdot \nabla \boldsymbol{v}\right) = -\nabla p + \mu \nabla^2 \boldsymbol{v} + \boldsymbol{f} - \frac{\mu}{K}\boldsymbol{v} - \frac{C_E}{K^{1/2}}\rho |\boldsymbol{v}| \boldsymbol{v} \tag{3.2}$$

K is the permeability of the porous medium which is calculated by the Carman-Kozeny equation, and C_E is the Ergun constant [30], [32].

$$K = \frac{1}{180}\frac{e^3}{(1-e)^2} D_s^2 \tag{3.3}$$

$$C_E = \frac{1.8}{(180e^5)^{1/2}} \tag{3.4}$$

D_s is the particle size and e is the porosity. K is independent of the fluid flow properties and only depends on the geometry of the medium.

In the present work, the maximum Reynolds number is below 200, thus we assume that the flow is laminar. The body force is neglected, and we simplify the equation for unidimensional flow as follows, where u_D is Darcy velocity in the axial direction.

$$\frac{\rho_f}{e}\left(\frac{\partial u_D}{\partial \tilde{t}}\right) = -\frac{\partial p}{\partial \tilde{x}} - \frac{\mu_f}{K}u_D - \frac{C_E \rho_f}{K^{1/2}}|u_D|u_D \tag{3.5}$$

3.2 Thermodynamics Model

A 1-D transient model is used to analyze the thermal performance of the regenerator under the following assumptions.

- Heat conduction in the radial direction is infinite.
- Heat leak to the surroundings is negligible.
- The physical properties of the heat transfer fluid and the matrix material are constant (except the specific heat of gadolinium) and determined based on the average temperature.
- The solid matrix is equally distributed and the porosity is homogeneous

3.2.1 Fluid Domain

Figure 3-1 shows the energy balance in a control volume in the regenerator domain.

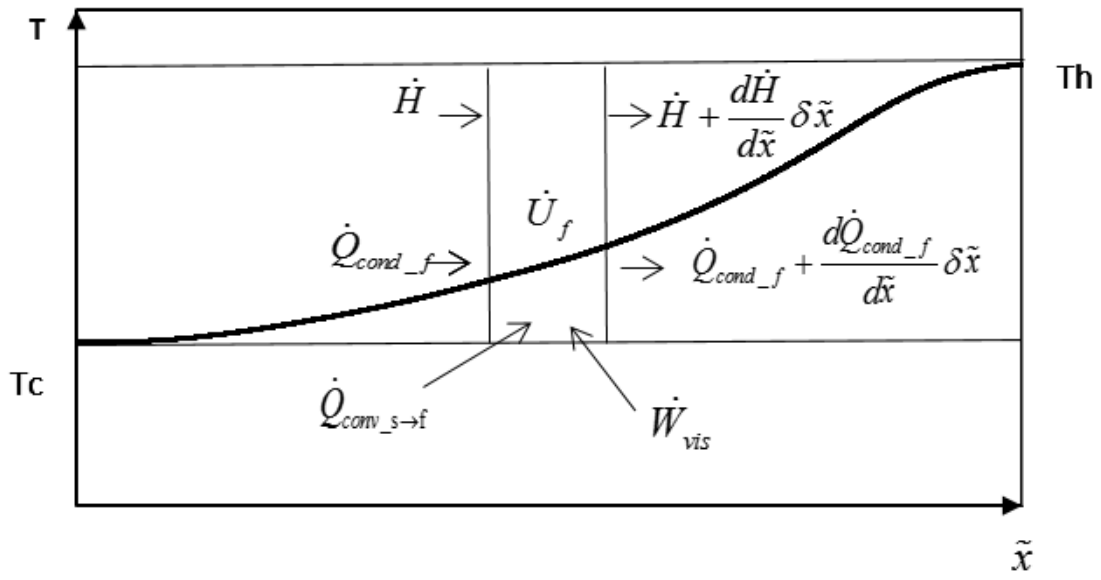

Figure 0-1 Energy balance for the fluid in a control volume in the regenerator includes internal energy, enthalpy flux, heat conduction, convection and viscous dissipation.

Energy change rate = Enthalpy flux + Heat conduction +Heat Convection + Viscous dissipation

This equation can be written as below.

$$\dot{U}_f = \dot{Q}_{flux} + \dot{Q}_{cond\_f} + \dot{Q}_{conv\_f} - \dot{W}_{vis} \tag{3.6}$$

Each term in the equation can be calculated as

$$\dot{U}_f = \rho_f A_f c_f \frac{\partial T_f}{\partial \tilde{t}} \tag{3.7}$$

$$\dot{Q}_{flux} = -\dot{m} c_f \frac{\partial T_f}{\partial \tilde{x}} \tag{3.8}$$

$$\dot{Q}_{cond\_f} = \frac{\partial}{\partial \tilde{x}}\left(k_f A_f \frac{\partial T_f}{\partial \tilde{x}}\right) \tag{3.9}$$

$$\dot{Q}_{conv\_f} = h_f P_w (T_s - T_f) \tag{3.10}$$

$$\dot{W}_{vis} = \frac{\dot{m}}{\rho_f}\frac{dp}{dx} \tag{3.11}$$

c_f the specific heat of fluid, $\dot{m}$ the mass flow rate, L the length of regenerator, k_f the conductivity of fluid, A_f the flow area in the regenerator, h_f the convection coefficient between the fluid and solid, P_w the wetted perimeter. Often, the viscous dissipation is neglected due to its small influence in the energy balance. Thus, in the case of a negligible viscous term we have the energy balance equation for the regenerator fluid as below.

$$\rho_f A_f c_f \frac{\partial T_f}{\partial \tilde{t}} = -\dot{m} c_f \frac{\partial T_f}{\partial x} + \frac{\partial}{\partial x}(k_f A_f \frac{\partial T_f}{\partial x}) + h_f P_w (T_s - T_f) \tag{3.12}$$

3.2.2 Solid Domain

According to conservation of energy, we have the energy balance for the stationary solid matrix as following.

Energy change rate =Heat conduction + Convection

That is

$$\dot{U}_s = \dot{Q}_{cond\_s} + \dot{Q}_{conv\_s} \tag{3.13}$$

Each term in the equation can be calculated as below.

$$\dot{U}_s = \rho_s A_s c_s \frac{\partial T_s}{\partial \tilde{t}} \tag{3.14}$$

$$\dot{Q}_{cond\_s} = \frac{\partial}{\partial \tilde{x}}(k_s A_s \frac{\partial T_s}{\partial \tilde{x}}) \tag{3.15}$$

$$\dot{Q}_{conv\_s} = h_f P_w (T_f - T_s) \tag{3.16}$$

In the equations above, A_s is the solid area of the regenerator, c_s is the specific heat capacity of the solid material, and k_s is the conductivity of the solid material.

Substituting them into Equation 3.13, and we have

$$\rho_s A_s c_s \frac{\partial T_s}{\partial \tilde{t}} = \frac{\partial}{\partial x}(k_s A_s \frac{\partial T_s}{\partial x}) + h_f P_w (T_f - T_s) \tag{3.17}$$

3.2.3 Effective Thermal Conductivity

The one-dimensional model of the regenerator cannot capture the radial mixing of the fluid due to tortuosity. Furthermore, the microstructure of the solid matrix is not resolved so point contacts and geometrical influences on diffusion are not resolved. These phenomena are approximated using a correlation developed by Hadley, as shown in Equation 3.18 and 3.21, to account for the static and dynamic conduction in the regenerator [33].

k_{static} is an effective coefficient for the conductivity of the regenerator combining the fluid and solid properties.

$$k_{static} = k_f[(1-\alpha_0)\frac{ef_0 + \frac{k_s}{k_f}(1-ef_0)}{1-e(1-f_0)+\frac{k_s}{k_f}e(1-f_0)} + \alpha_0\frac{2(\frac{k_s}{k_f})^2(1-e)+(1+2e)\frac{k_s}{k_f}}{(2+\alpha)\frac{k_s}{k_f}+1-e}] \tag{3.18}$$

where

$$f_0 = .8 + .1e \tag{3.19}$$

$$\log\alpha_0 = -1.084 - 6.778(e-0.298) \quad 0.298 < e < 0.580 \tag{3.20}$$

This effective static conductivity coefficient is used in the conduction term in the energy equation for the solid (k_s=k_{static}).

$k_{dynamic}$ accounts for the fluid dispersion in the regenerator, for packed beds using spherical particles, it is calculated as below [30].

$$k_{dynamic} = 0.75ek_f R_{e_h} P_r \tag{3.21}$$

R_{e_h} is Reynolds number based on hydraulic diameter of the regenerator and P_r is Prandtl number. This effective dynamic conductivity coefficient is used as the conduction term in the regenerator fluid equation (k_f=$k_{dynamic}$).

3.2.4 Effective Heat Convection Coefficient

The heat convection between the regenerator fluid and solid is determined by the Nusselt number correlation developed by Wakao and Kaguei [34], [35], with a Reynolds number which is calculated based on the spherical particle size and superficial velocity [36].

$$h_f = N_u \frac{k_f}{D_s} \tag{3.22}$$

$$N_u = 2 + 1.1 R_{e_p}^{\ 0.6} P_r^{1/3} \tag{3.23}$$

R_{e_p} is the Reynolds number based on the sphere diameter.

$$R_{e_p} = \frac{\dot{m} D_p}{A_c \mu} \tag{3.24}$$

A degradation factor developed by Engelbrecht is used to account for the temperature gradients within a particle [37].

$$\beta = 1 - \frac{4}{35 F_o} \tag{3.25}$$

F_o is the Fourier number, which is the ratio of diffusive transport rate by the quantity storage rate, calculated as below.

$$F_o = \frac{k_s}{\rho_s c_{p_s} f (\frac{D_s}{2})^2} \tag{3.26}$$

Using the degradation factor we have the effective heat convection coefficient calculated as below.

$$h_{eff} = \frac{h}{1 + \frac{\mathrm{Bi}}{5} \beta} \tag{3.27}$$

B_i is the Biot number.

$$B_i = \frac{N_u k_f}{2k_s} \tag{3.28}$$

3.2.5 Dead Volumes

To account for the parasitic dead volume in the experimental system, the model includes domains where there is no solid matrix. This dead volumes are located between the heat exchanger and the regenerator.

As shown in Figure 1-1, two sections of dead volume exist at the ends of the regenerator, with the same diameter as the regenerator itself.

The energy balance for the fluid in the dead volume is as follows.

Energy change rate =Enthalpy flux + Convection

That is

$$\dot{U}_{dv\_f} = \dot{Q}_{dv\_flux} + \dot{Q}_{dv\_cond\_f} + \dot{Q}_{dv\_conv\_f} \tag{3.29}$$

For each term

$$\dot{U}_{dv\_f} = \rho_f A_{dv\_f} c_f \frac{\partial T_f}{\partial \tilde{t}} \tag{3.30}$$

$$\dot{Q}_{dv\_flux} = -\dot{m} c_f \frac{\partial T_f}{\partial x} \tag{3.31}$$

$$\dot{Q}_{dv\_cond\_f} = \frac{\partial}{\partial x}(k_f A_c \frac{\partial T_f}{\partial x}) \tag{3.32}$$

$$\dot{Q}_{dv\_conv\_f} = \frac{(T_{amb} - T_f)}{R_{dv} L_{dv}} \tag{3.33}$$

A_{dv_f} is the fluid area in each dead volume, L_{dv} is the length of each dead volume, and R_{dv} is the total thermal resistance between the dead volume and the ambient environment.

In order to determine the value of R_{dv}, a thermal circuit is assumed to consist of tube wall, outer insulation, and an external convection resistance as shown in Figure 3-2.

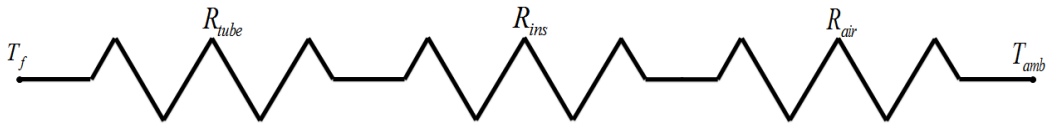

Figure 0-2 Thermal circuit for dead volume includes thermal resistances of tube, thermal insulation and air.

Each thermal resistance is calculated as below.

$$R_{tube} = \frac{\ln(D_o / D_i)}{2\pi k_{tube} L_{dv}} \tag{3.34}$$

$$R_{ins} = \frac{\ln(D_{os} / D_o)}{2\pi k_{ins} L_{dv}} \tag{3.35}$$

$$R_{air} = \frac{1}{\pi Nu_{air} k_{air} L_{dv}} \tag{3.36}$$

D_o and D_i are the outer and inner diameters of the tube respectively, D_{os} is the outer diameter of the insulation foam. The conductivity coefficients of each part and the Nusselt number of air are obtained from published literature [38].

After substitution, the energy equation for the dead volume is as follows.

$$\rho_f A_{dv\_f} c_f \frac{\partial T_f}{\partial \tilde{t}} = -\dot{m}c \frac{\partial T_f}{\partial x} + \frac{\partial}{\partial x}(k_f A_c \frac{\partial T_f}{\partial x}) + \frac{(T_{amb} - T_f)}{R_{dv} L_{dv}} \tag{3.37}$$

3.2.6 Boundary Conditions

The direction of the flow changes during a full operating cycle while the inlet temperature may also vary, leading to a time dependent boundary condition.

When the fluid flows from cold heat exchanger into the regenerator, during the time period of $\tilde{t} \leq \tau_b$, the boundary condition is as follows.

$$T_f = T_{CHEX} \quad \text{, at} \quad x = 0 \tag{3.38}$$

$$\frac{\partial T_f}{\partial x} = 0 \quad \text{, at} \quad x = L_{reg} \tag{3.39}$$

T_{CHEX} represents the fluid temperature from the cold heat exchanger.

When the flow direction is changed, the fluid flows from hot heat exchanger into the regenerator, during the time period of $\tau_b < \tilde{t} \leq 2\tau_b$, and the boundary condition becomes as below.

$$T_f = T_{HHEX} \quad \text{, at} \quad x = L_{reg} \tag{3.40}$$

$$\frac{\partial T_f}{\partial x} = 0 \quad \text{, at} \quad x = 0 \tag{3.41}$$

T_{HHEX} represents the fluid temperature from the hot heat exchanger.

Here we consider the problem of the regenerator with periodic flow reversal and sinusoidal mass flow during each blow. A linear temperature profile between T_{CHEX} and T_{HHEX} for solid and fluid is assumed for initial conditions.

3.2.7 Non-Dimensionalization

Time is non-dimensionalized using the blow period.

$$t = \frac{\tilde{t}}{\tau_B} \tag{3.42}$$

And the regenerator length is used to normalize the spatial parameter.

$$x = \frac{\tilde{x}}{L_{reg}} \tag{3.43}$$

Thus, the governing equations of the fluid and solid domains become as

$$\rho_f A_f c_f \frac{\partial T_f}{\partial t} = -\frac{\dot{m} c_f \tau_b}{L_{reg}} \frac{\partial T_f}{\partial x} + \frac{\tau_b}{L_{reg}^2} \frac{\partial}{\partial x}(k_{dynamic} A_f \frac{\partial T_f}{\partial x}) + h_{eff} P_w \tau_b (T_s - T_f) \quad (3.44)$$

$$\rho_s A_s c_s \frac{\partial T_s}{\partial t} = \tau_b \frac{1}{L_{reg}^2} \frac{\partial}{\partial x}(k_{static} A_s \frac{\partial T_s}{\partial x}) + h_{eff} P_w \tau_b (T_f - T_s) \quad (3.45)$$

where *x* and *t* are non-dimensional space and time. To develop standard parameters governing regenerator operation, both equations are normalized by thermal capacity of the solid matrix.

$$\frac{m_f c_f}{m_s c_s} \frac{\partial T_f}{\partial t} = -\frac{\dot{m} c_f \tau_b}{m_s c_s} \frac{\partial T_f}{\partial x} + \frac{\partial}{\partial x}(\frac{k_{dynamic} A_f \tau_b}{m_s c_s L_{reg}} \frac{\partial T_f}{\partial x}) + \frac{h_{eff} A_w \tau_b}{m_s c_s}(T_s - T_f) \quad (3.46)$$

$$\frac{\partial T_s}{\partial t} = \frac{\partial}{\partial x}(\frac{k_{static} A_s \tau_b}{m_s c_s L_{reg}} \frac{\partial T_s}{\partial x}) + \frac{h_{eff} A_w \tau_b}{m_s c_s}(T_f - T_s) \quad (3.47)$$

Thus, the governing equations for the fluid and solid become as below.

$$R \frac{\partial T_f}{\partial t} = -\Phi \frac{\partial T_f}{\partial x} + \frac{\partial}{\partial x}(K_f \frac{\partial T_f}{\partial x}) + NTU \cdot \Phi (T_s - T_f) \quad (3.48)$$

$$\frac{\partial T_s}{\partial t} = \frac{\partial}{\partial x}(K_s \frac{\partial T_s}{\partial x}) + NTU \cdot \Phi (T_f - T_s) \quad (3.49)$$

where *R* is the thermal capacity ratio between entrained fluid and solid, Φ is utilization, K_f and K_s are the effective conductivities in fluid and solid respectively, and *NTU* is *number of transfer units* [28], [39].

$$R = \frac{m_f c_f}{m_s c_s} \quad (3.50)$$

$$NTU = \frac{h_{eff} \cdot A_w}{\dot{m} c_f} \quad (3.51)$$

For the dead volume, after non-dimensionalization using blow period and regenerator length the fluid equation becomes:

$$\frac{\rho_f V_{dv\_f} c_f}{m_s c_s}\frac{\partial T_f}{\partial t} = \frac{-\dot{m} c_f \tau_b L_{dv}}{m_s c_s L_{reg}}\frac{\partial T_f}{\partial x} + \frac{\partial}{\partial x}\left(\frac{k_f A_c \tau_b L_{dv}}{m_s c_s L_{reg}^2}\frac{\partial T_f}{\partial x}\right) + \frac{m_{dis} c_f}{m_s c_s}\frac{\tau_b}{R_{dv} m_{dis} c_f}(T_{amb} - T_f)$$

(3.52)

After simplification, it is

$$R_{dv}\frac{\partial T_f}{\partial t} = -\Phi_{dv}\frac{\partial T_f}{\partial x} + \frac{\partial}{\partial x}(K_{dv}\frac{\partial T_f}{\partial x}) + NTU_{dv}\Phi(T_{amb} - T_f) \tag{3.53}$$

where

$$R_{dv} = \frac{\rho_f V_{dv\_f} c_f}{m_s c_s} \tag{3.54}$$

$$\Phi_{dv} = \frac{\dot{m} c_f \tau_b L_{dv}}{m_s c_s L_{reg}} \tag{3.55}$$

$$K_{dv} = \frac{k_f A_c \tau_b L_{dv}}{m_s c_s L_{reg}^2} \tag{3.56}$$

and

$$NTU_{dv} = \frac{\tau_b}{R_{dv} m_{dis} c_f} \tag{3.57}$$

In this chapter, simplified physical models are developed to describe the momentum and energy balances in the current passive regenerator tests. All experimental results will be presented in the next chapter.

Experimental Results

In this chapter, the results of the passive experiments conducted on stainless steel, lead and gadolinium beds are presented and discussed.

4.1 Pressure Drop

The data collected by the two pressure transducers is processed to obtain the pressure drop through the regenerator beds. The instantaneous pressure drop measurements of the three matrices present similar sinusoidal waveforms. The uncertainty of the estimated pressure drop measurements is 15.0 kPa, based on the reported uncertainty for the transducers in use. In Figure 4-1, a set of pressure data and the simultaneous displacement data from a test are plotted.

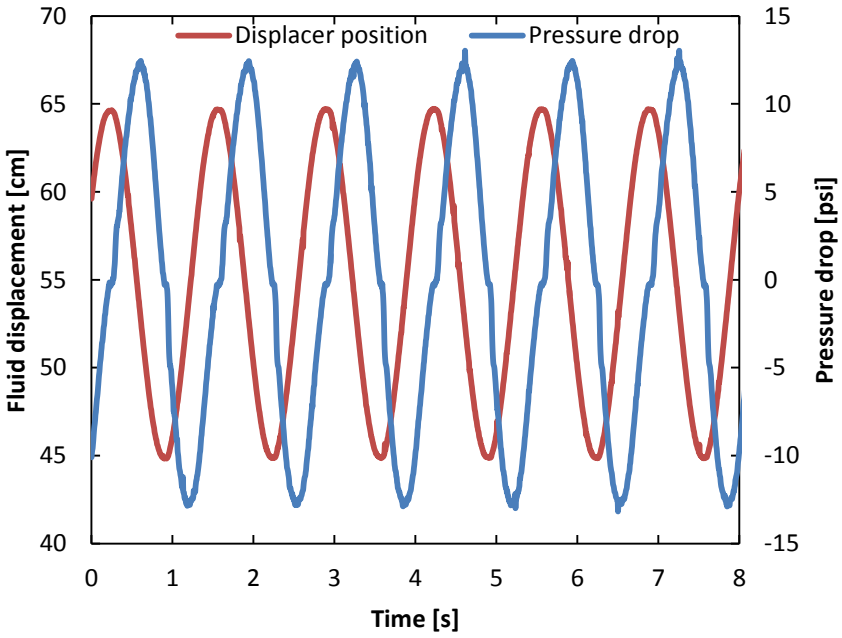

Figure 0-1 Pressure drop through the regenerator is measured using two pressure transducers, and according position of the displacer is recorded by the linear potentiometer, using gadolinium bed with displaced fluid volume of 13.9 cm^3 and operating frequency of 0.75 Hz.

To show the phase relation between the pressure and the fluid displacement clearly, two parameters are normalized by their own amplitudes, as shown in Figure 4-2. The measurements start from the minimum displacement.

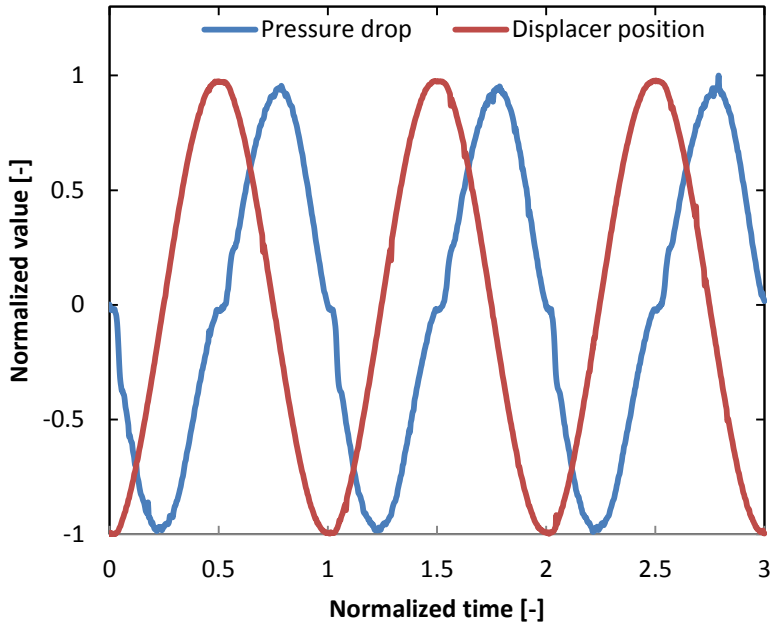

Figure 0-2 Data in Figure 4-1 is simplified and normalized to show the relation between the pressure drop and the displacer position.

The phase relation between the two signals agrees with expected behavior for pressure drop under a low-frequency sinusoidal-form oscillating flow. When the displacer position reaches 0 (the mean position, or, middle of the stroke), the flow velocity reaches its maximum value, leading to a peak of the pressure drop. The shoulders appearing in the pressure drop curve can be explained by backlash in the crank mechanism. The small discrepancy between the negative and positive peaks in both the pressure drop and displacement can be a result of the limited instruments accuracy and lack of symmetry between the hot blow and cold blow.

The experimental average pressure drop results for the three regenerator listed in Table 2-2 are shown in Figure 4-3, 4-4 and 4-5, using Equation 2.14.

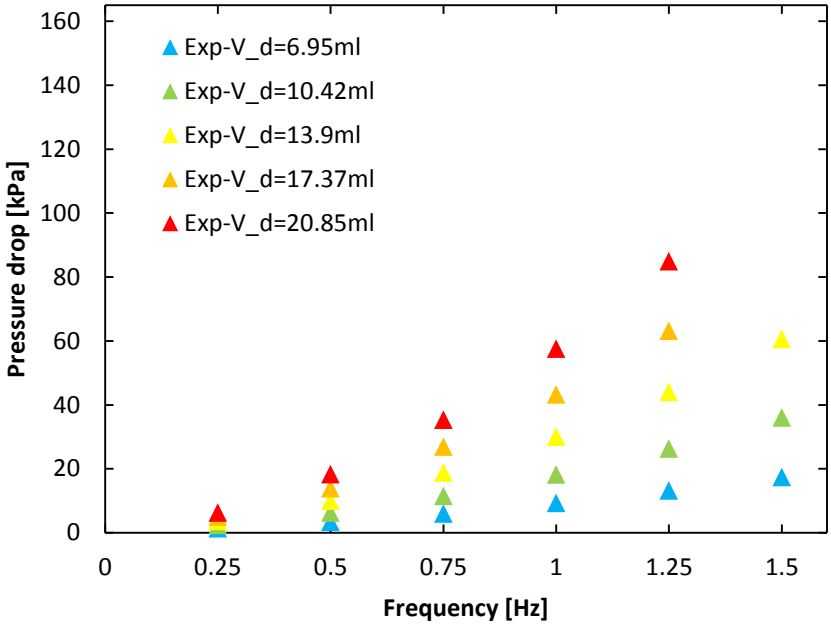

Figure 0-3 Experimental data of pressure drop for stainless steel spheres bed is presented as a function of frequency and displaced volume.

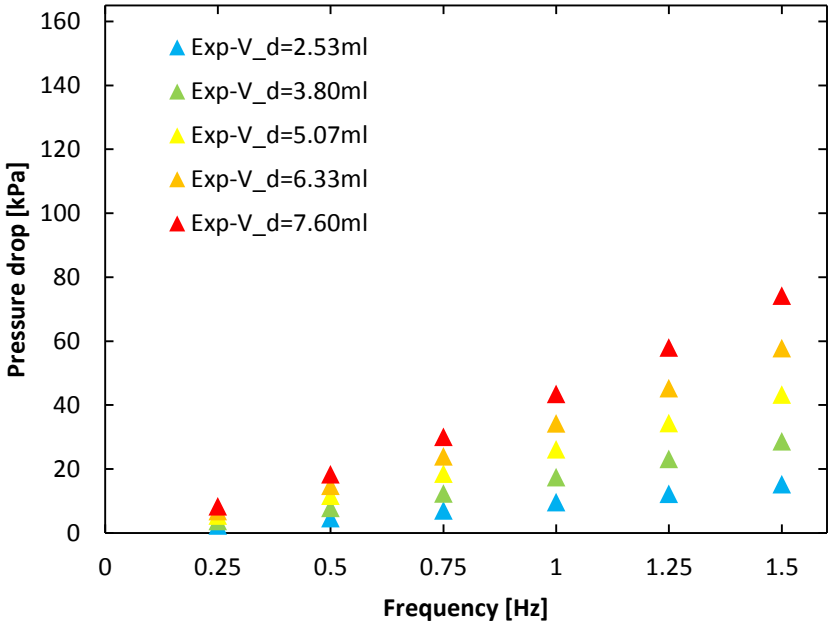

Figure 0-4 Experimental data of pressure drop for lead spheres bed is presented as a function of frequency and displaced volume.

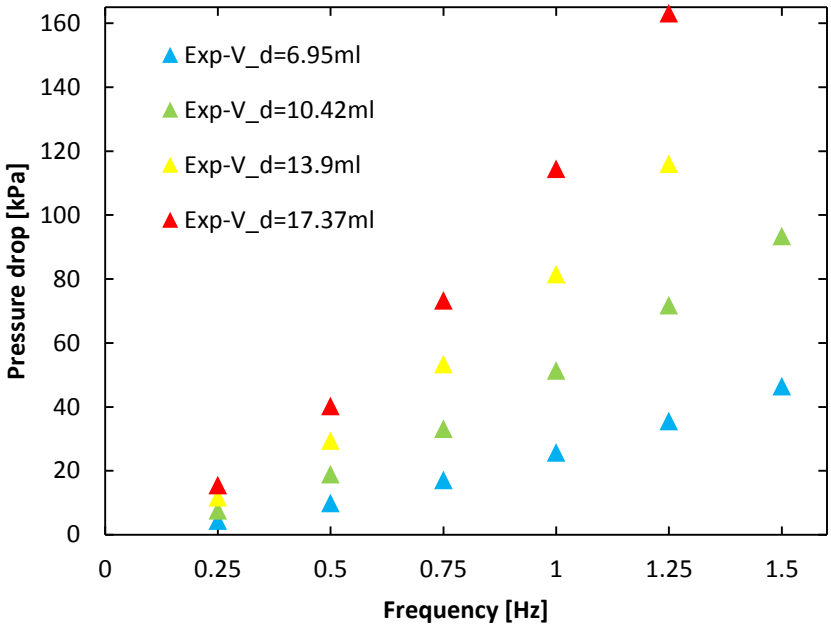

Figure 0-5 Experimental data of pressure drop for gadolinium spheres bed is presented as a function of frequency and displaced volume.

From the figures above, we can see that the pressure drop exhibits a quasi-parabolic behavior with respect to frequency, due to the fact that superficial velocity increases linearly with frequency. The highest average pressure drop takes place in the gadolinium bed, and lowest in the lead bed. This is due to the smaller displaced volumes used for the lead matrix tests than the other two sets of tests. Thus for the same frequency the mass flow rates for the lead bed tests are much smaller. In addition, the diameter of the gadolinium spheres is smaller than that of the stainless steel spheres, leading to a lower permeability for the gadolinium bed, hence higher pressure drops occur.

Tests with a displaced volume of 20.9 cm^3 are not performed on the gadolinium bed, due to the high pressure drop and the minimum and maximum allowable working pressures of the device. A similar situation occurs with the stainless steel bed and 1.5 Hz tests are not possible for the scenarios with the two biggest displaced fluid volumes.

4.2 Temperature Span and Variation

Figure 4-6 shows the instantaneous temperature measurements at the seven locations inside the gadolinium regenerator for a displaced fluid volume of 13.9 cm^3 and a frequency of 0.75 Hz.

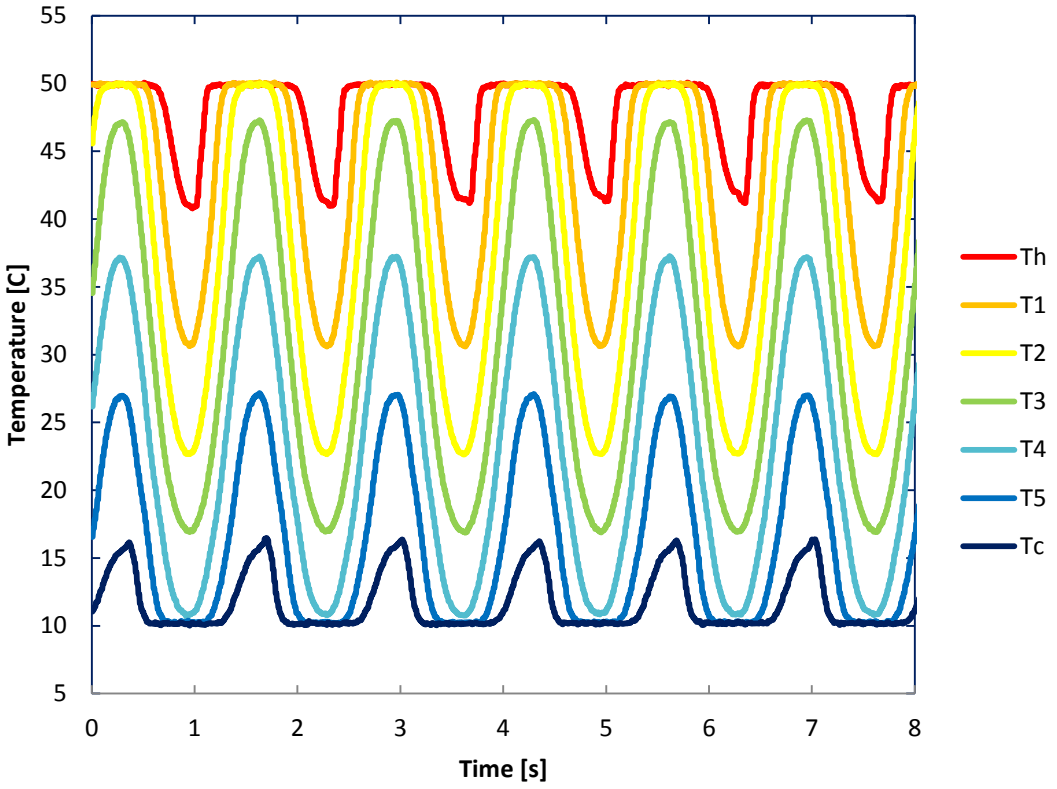

Figure 0-6 Temperature variations are measured at seven locations, using gadolinium regenerator bed with displaced fluid volume of 13.9 cm^3 and operating frequency of 0.75 Hz.

Most internal temperature profiles are approximately sinusoidal, and the loss of symmetry in the temperature profiles at both ends is due to the fluid entering the regenerator from the constant-temperature heat exchangers and because of dead volume effect.

For any location in the regenerator the minimum and maximum temperatures arise at the end of the cold blow and hot blow respectively. The measured extremum temperatures for each measured location in the stainless steel regenerator beds with operating frequency of 0.25 Hz and 1.25 Hz are shown in Figure 4-7.

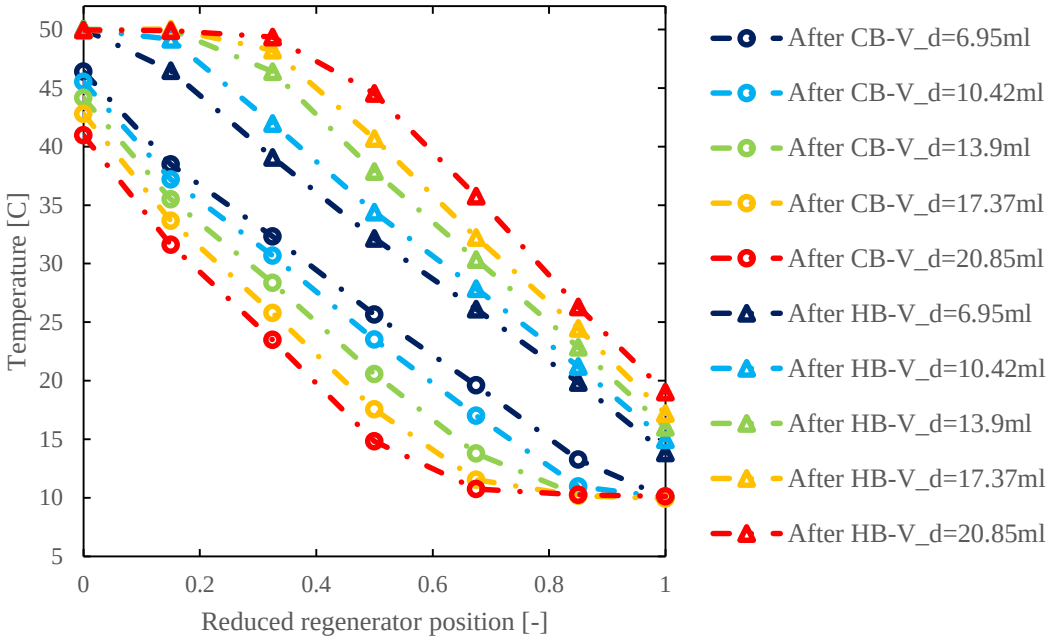

(a)

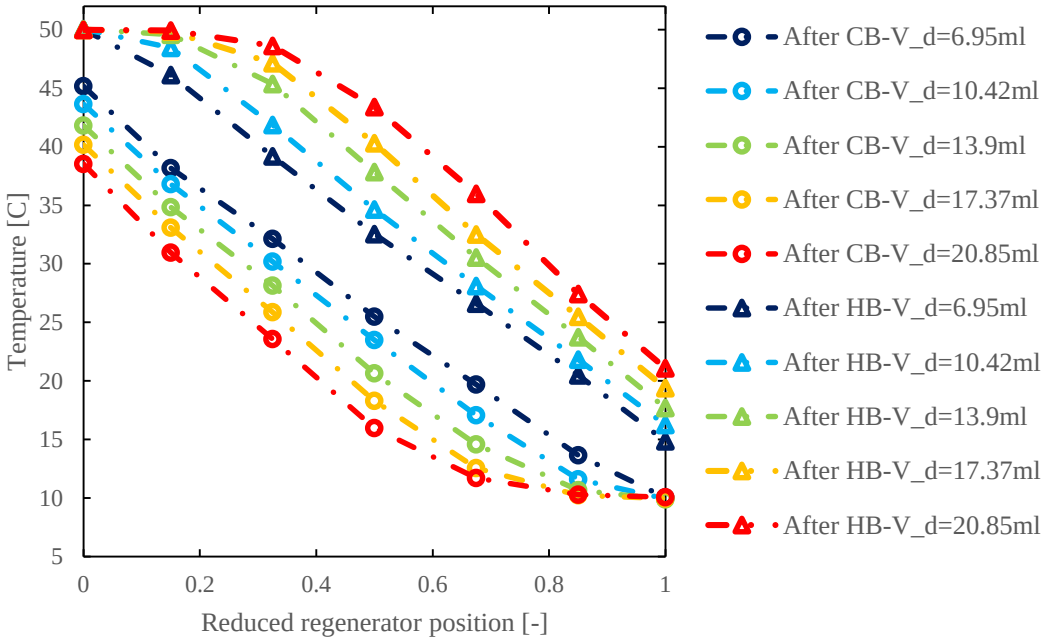

(b)

Figure 0-7 Longitudinal temperature distributions after cold blow and after hot blow for stainless steel spheres bed tests are presented as a function of reduced regenerator position and displaced volume, (a) 0.25Hz frequency, (b) 1.25 Hz frequency.

As we can see in the figure above, with a certain utilization, the temperature distribution after cold blow and that after hot blow are almost symmetric for the

stainless steel bed, due to the nearly constant specific heat capacity of the material through the temperature range. The area between the cold-blow curve and hot-blow curve increases with utilization, indicating that the fluid from the heat exchangers penetrates further into the regenerator matrix. However, higher penetration of the fluid from one side enlarges the temperature difference between the outlet fluid and the adjacent heat exchanger fluid on the other side, leading to a decrease of the regenerator effectiveness. For an ideal regenerator with 100% effectiveness, there is no difference between the fluid temperatures at either end of the regenerator.

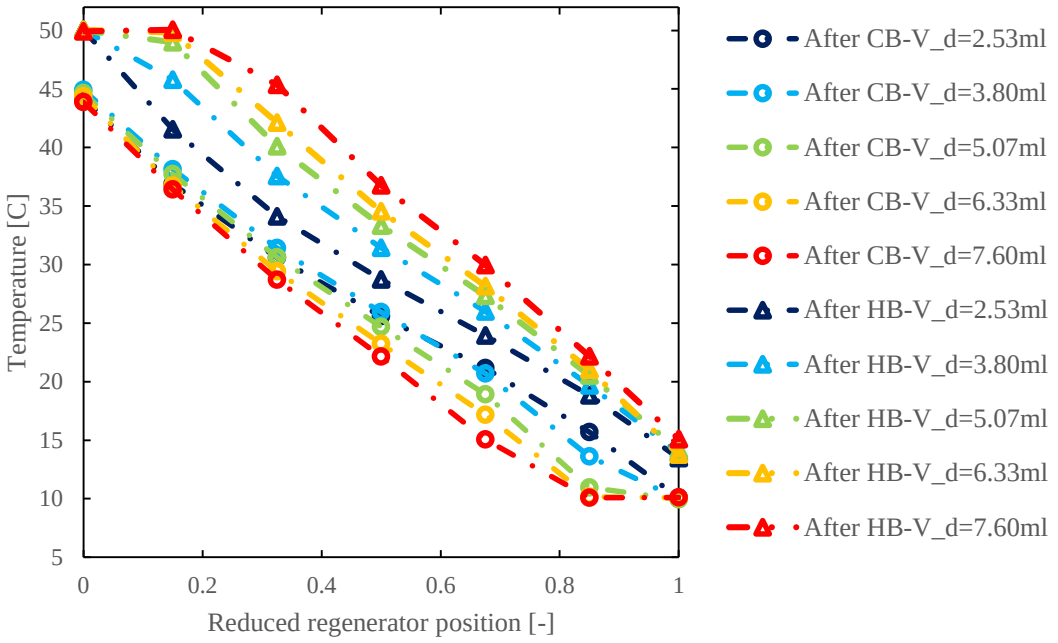

(a)

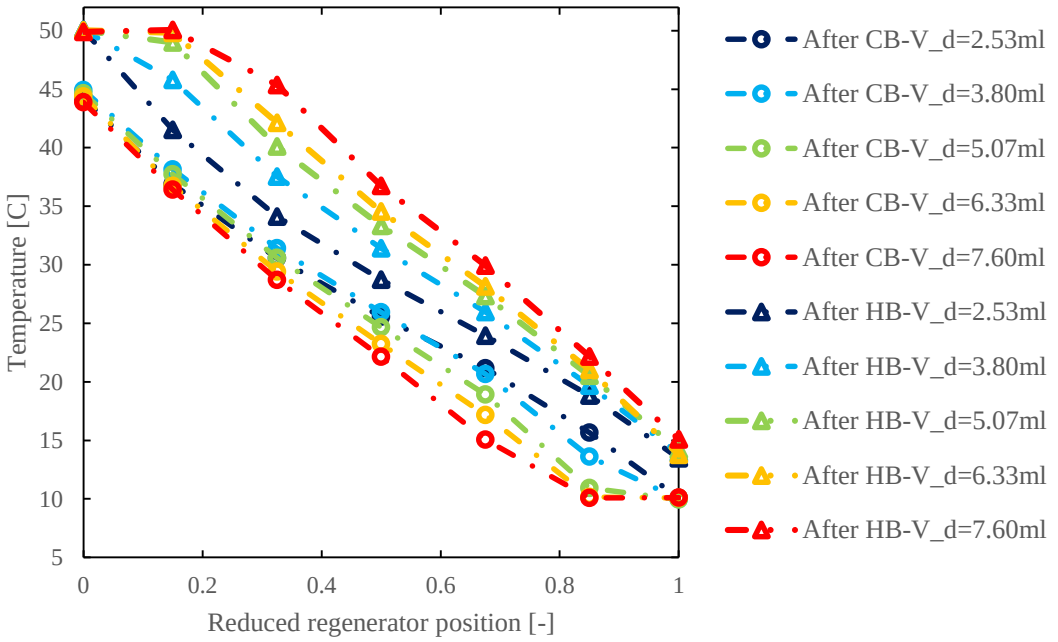

(b)

Figure 0-8 Longitudinal temperature distributions after cold blow and after hot blow for lead spheres bed tests are presented as a function of reduced regenerator position and displaced volume, (a) 0.25-Hz frequency, (b) 1.25-Hz frequency.

In the lead spheres bed tests shown in Figure 4-8, with an operating frequency of 1.25Hz, the longitudinal temperature distributions behave in a similar manner to the stainless steel tests, especially under large values of utilizations. Two different behaviors can be observed in the case of 0.25 Hz tests: (1) visible distortion shows up in the temperature profiles for the lowest utilizations and (2) the temperature profiles cross-over for the cold blow resulting in a higher exit temperature with increased utilization. One possibility is that this phenomenon results from the axial heat conduction, where at low Reynolds numbers the diffusion term becomes significant relative to the advection term.

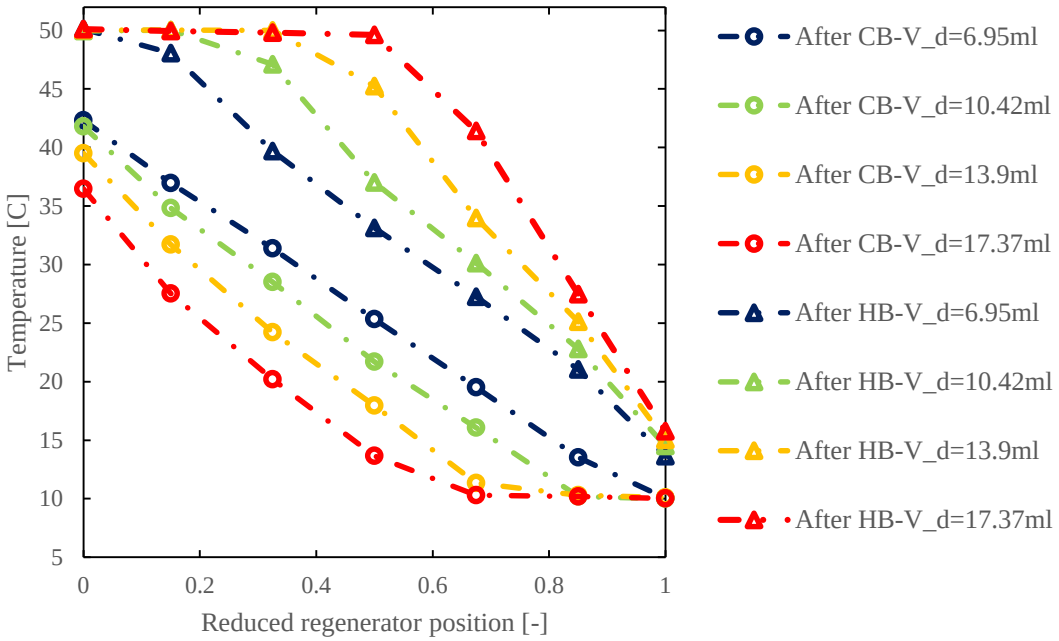

(a)

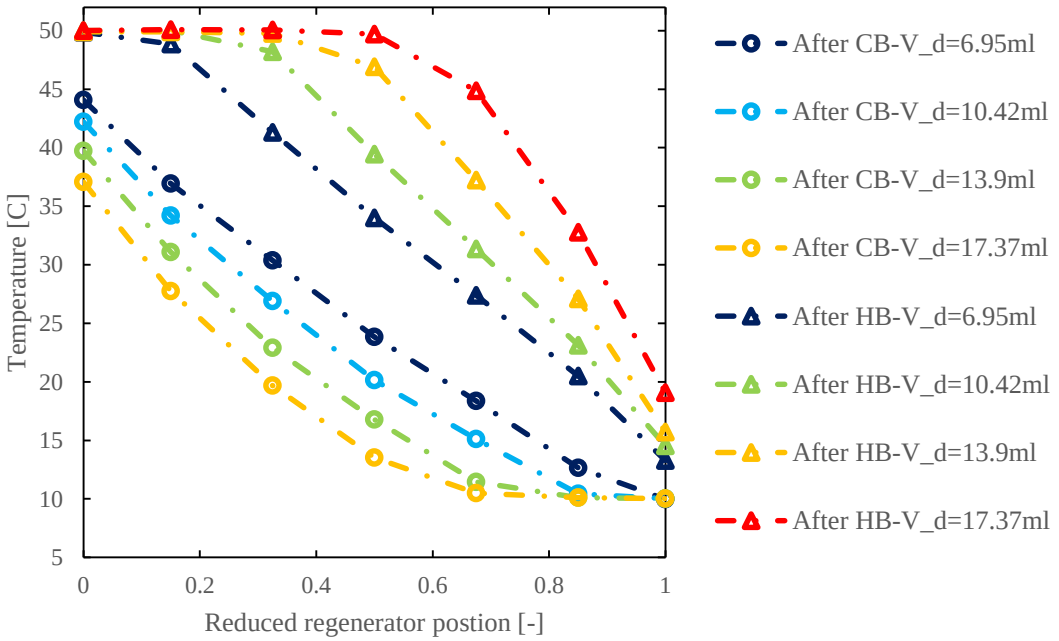

(b)

Figure 0-9 Longitudinal temperature distributions after cold blow and after hot blow for gadolinium bed tests are presented as a function of reduced regenerator position and displaced volume, (a) 0.25 Hz frequency, (b) 1.25 Hz frequency.

Figure 4-9 shows the measured temperature profiles for gadolinium spheres. Unlike lead and stainless steel, less symmetry is apparent between the cold-blow curves and the hot-blow curves. The temperature difference between the outlet fluid and the inlet fluid on the hot end is bigger than that at the cold end under high utilizations. This is due to the temperature dependence of the specific heat capacity of gadolinium, leading to a higher local utilization near the regenerator hot end than that near the cold end. This changing distribution of the thermal mass in the regenerator matrix results in different effectiveness of hot and cold blows.

4.3 Dead Volume Impact on the Inlet Temperature Profile

The fluid exiting the regenerator is either cooled down or heated up by the adjacent heat exchangers. Ideally, if there is no dead volume existing in the system, the fluid temperature should abruptly change from the exit temperature to the heat exchanger temperature when flow is reversed. However, the temperature profiles vary in a continuous manner throughout the cycle because of the dead volumes and the thermal effects including heat conduction and mixing that can arise during a flow reversal. Series of experiments are performed to examine dead volume impact on the inlet temperature profiles. Two additional experiments using gadolinium with varying dead volumes are performed. As a result, three dead volume conditions are explored with the same gadolinium bed. The dead volumes between the regenerator and the heat exchangers are estimated to be 2.0, 4.0 and 6.0 cm^3.

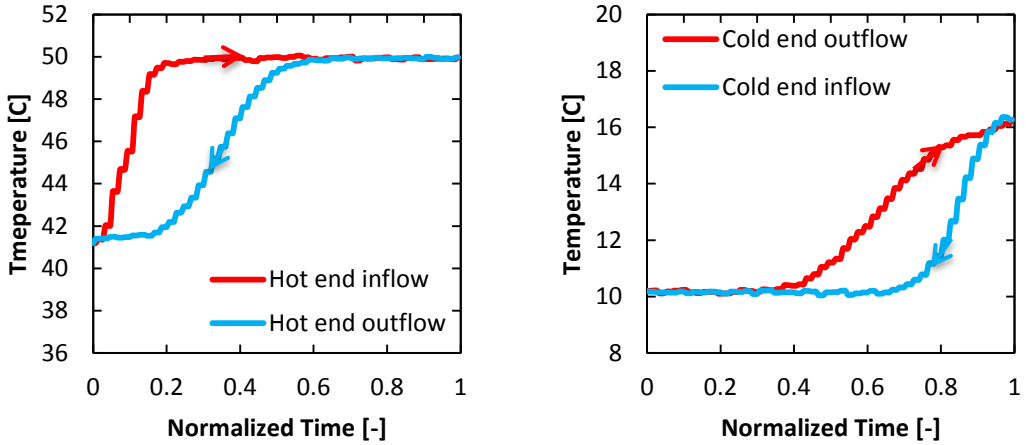

(a) (b)

Figure 0-10 Temperature variation on each end of regenerator is measured using gadolinium spheres regenerator, (a) hot end, (b) cold end, under displaced fluid volume of 13.9 cm^3 and frequency of 0.75 Hz, with dead volume of 2.0 cm^3.

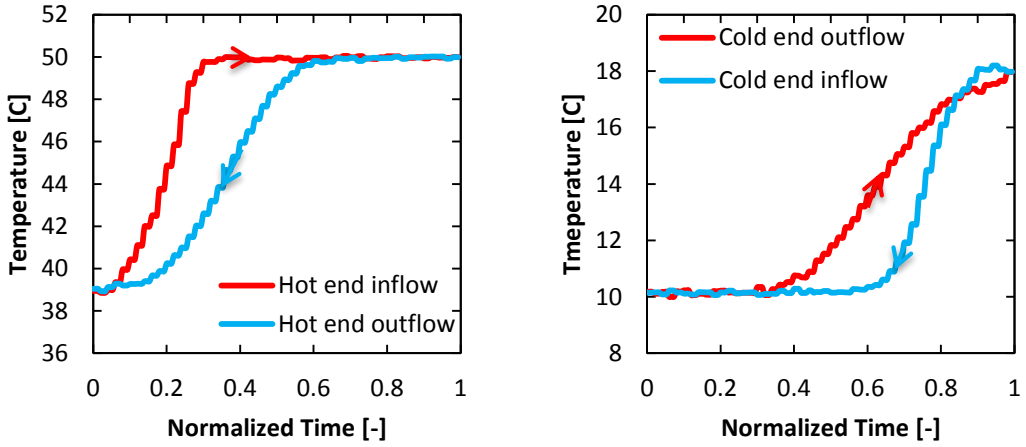

(a) (b)

Figure 0-11 Temperature variation on each end of regenerator is measured using gadolinium spheres regenerator, (a) hot end, (b) cold end, under displaced fluid volume of 13.9 cm^3 and frequency of 0.75 Hz, with dead volume of 4.0 cm^3.

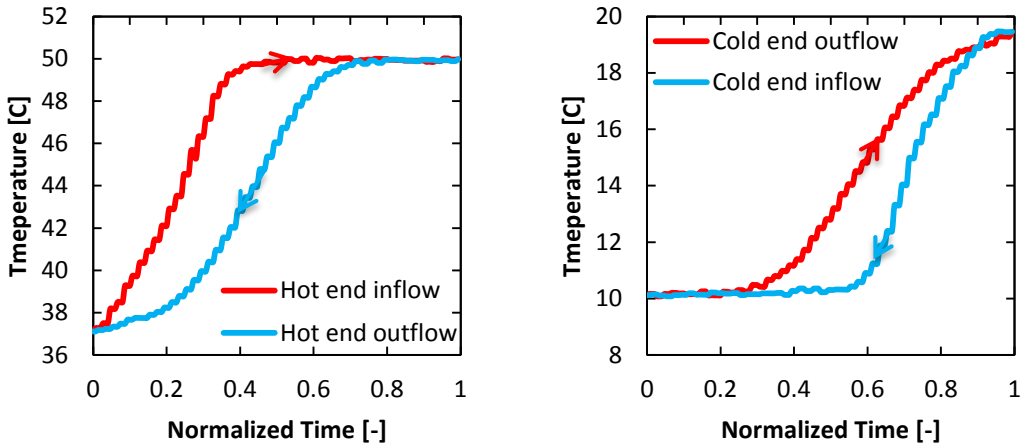

(a) (b)

Figure 0-12 Temperature variation on each end of regenerator is measured using gadolinium spheres regenerator, (a) hot end, (b) cold end, under displaced fluid volume of 13.9 cm^3 and frequency of 0.75 Hz, with dead volume of 6 cm^3.

As can be seen in Figure 4-10, with the minimum dead volume condition, the inflow temperatures for both ends of the regenerator are not the same as the heat exchanger temperatures. Increasing dead volume size shortens the fraction of a cycle when the outflow is in contact with the heat exchanger, causing an increase in the average difference between the inflow temperature and the corresponding heat exchanger temperature.

4.4 Regenerator Effectiveness

The effectiveness for each regenerator is determined using Equations 2.11 to 2.13, and the experimental data for temperature and mass flow rate.

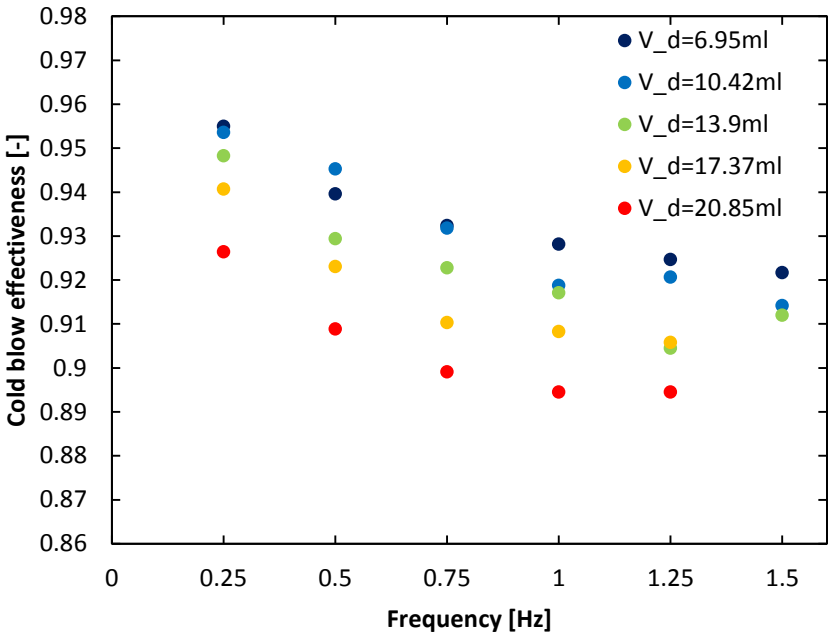

(a)

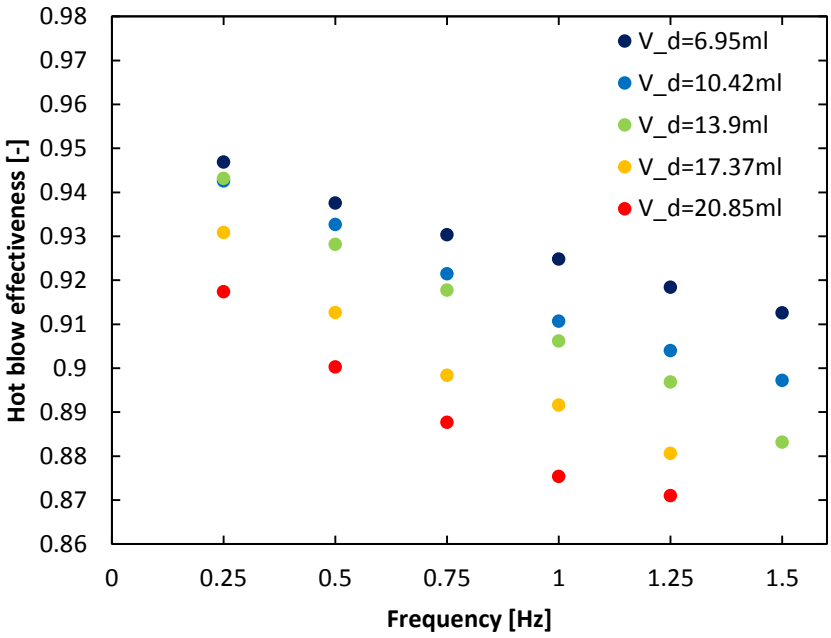

(b)

Figure 0-13 Effectiveness of stainless steel bed is presented as a function of frequency and displaced fluid volume, (a) cold blow, (b) hot blow.

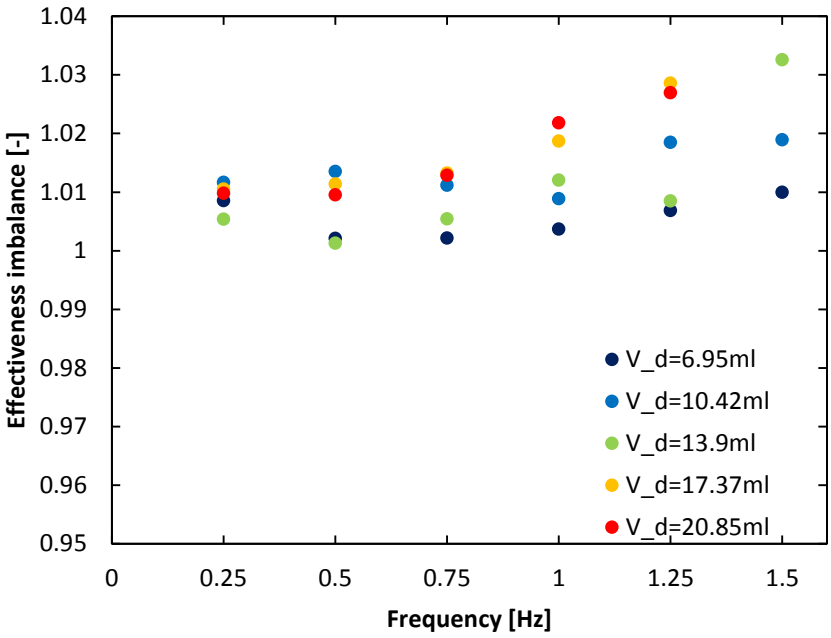

Figure 0-14 Effectiveness imbalance between hot blow and cold blow for stainless steel bed is presented as a function of frequency and displaced fluid volume.

As we can see, the effectiveness of the stainless steel bed decreases with increasing frequency under a constant utilization for both cold blow and hot blow. This behavior can be explained by basic regenerator theory where effectiveness decreases with decreasing NTU. NTU describes the ratio of the amount of heat transferred between the solid and the fluid to the fluid capacity rate. With a fixed displaced fluid volume, higher frequency leads to higher mass flow rate and smaller NTU. The convection coefficient is a function of mass flow rate with an exponential dependence where the exponent is less than one. So, although the numerator increases with flow rate, NTU decreases. And the two kinds of effectiveness present similar trends.

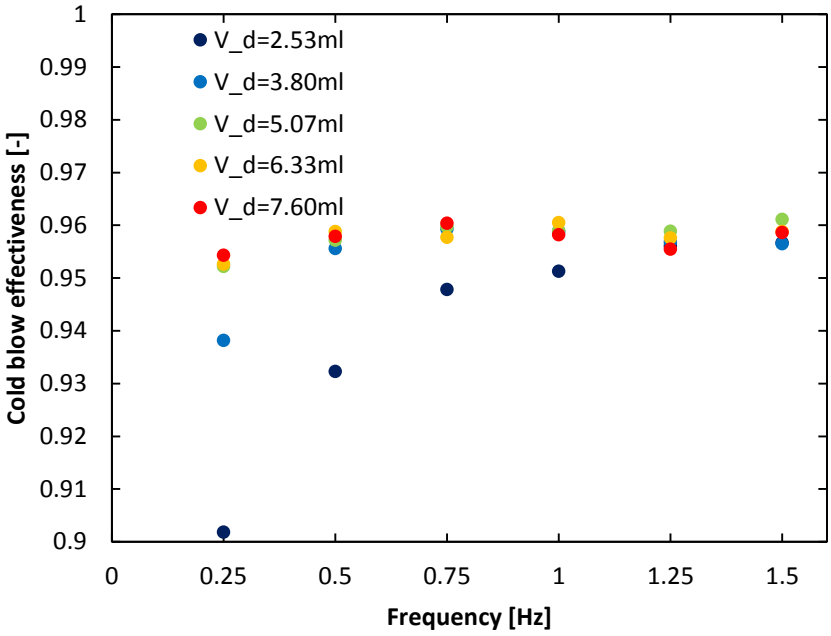

(a)

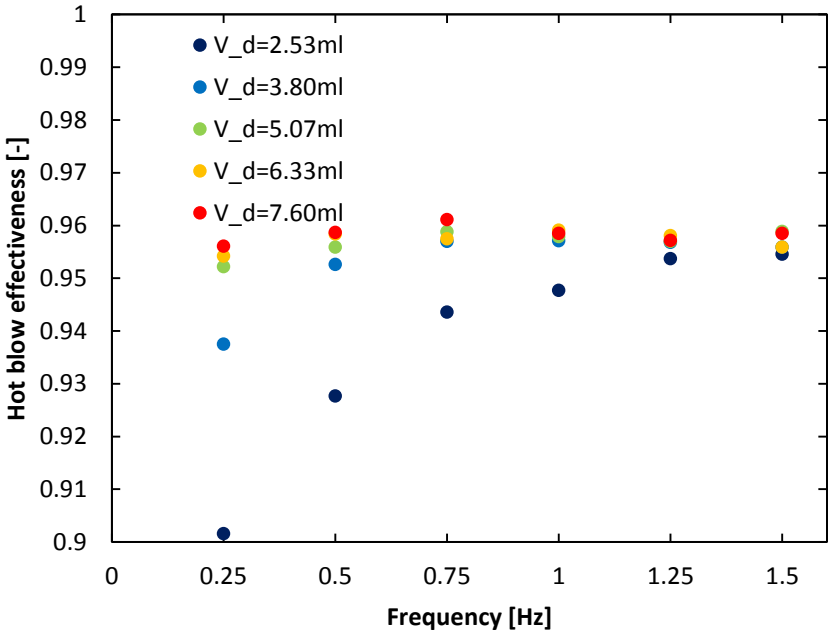

(b)

Figure 0-15 Effectiveness of lead bed is presented as a function of frequency and displaced fluid volume, (a) cold blow, (b) hot blow.

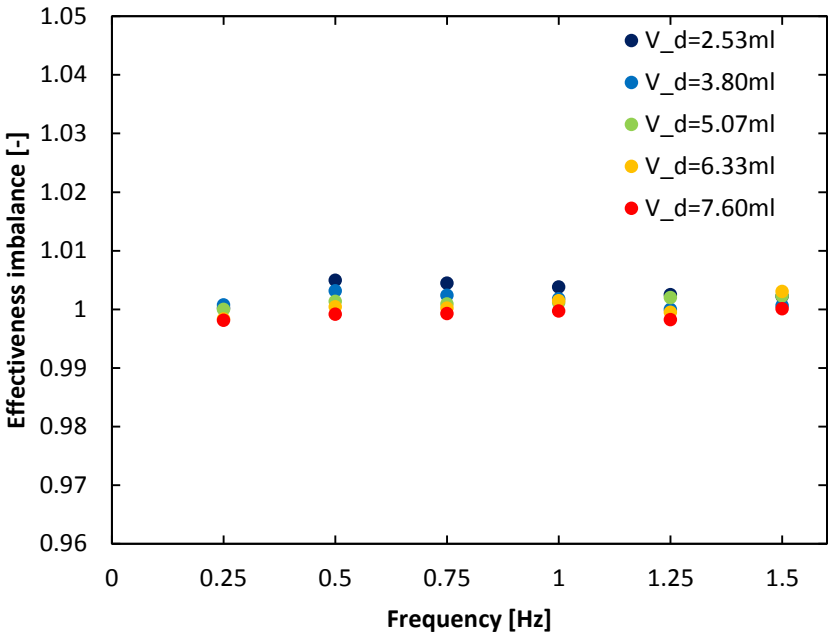

Figure 0-16 Effectiveness imbalance between hot blow and cold blow for lead bed is presented as a function of frequency and displaced fluid volume.

For the lead bed, the effectiveness behaves much differently, as shown in Figure 4-15 and 4-16. The effectiveness of both the cold blow and hot blow increase with frequency under constant displaced volume. One possible reason for this behavior is the impact of axial heat conduction losses. Another possibility is that the existence of the parasitic dead volume. One can imagine how the effect of a dead volume will be more significant as the displaced volume is decreased. Because the displaced volume is set by utilization, the tests on lead spheres use the smallest displacement and show lowest effectiveness.

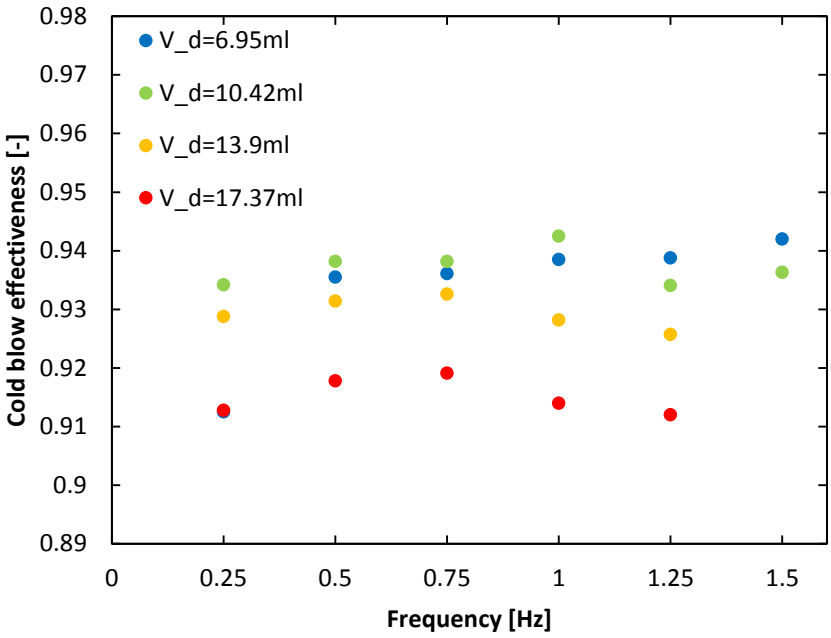

(a)

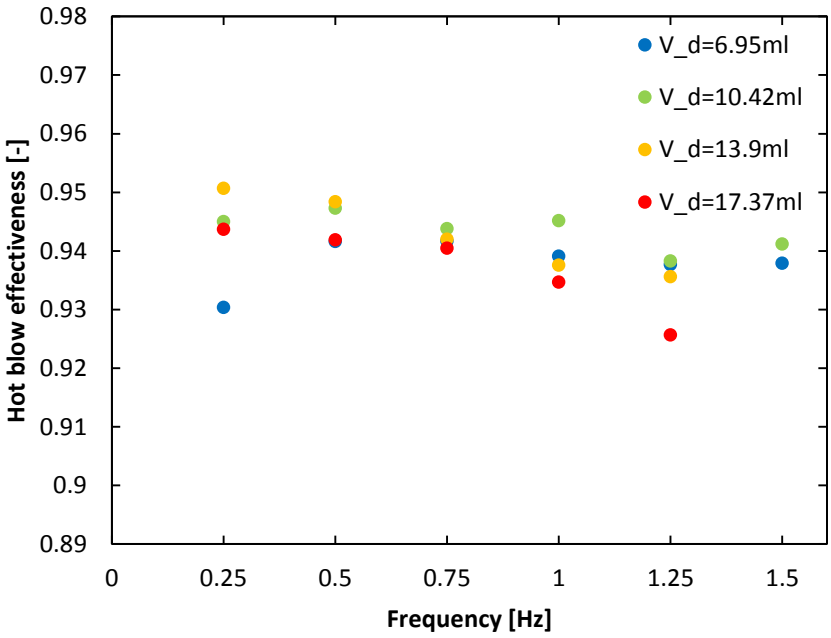

(b)

Figure 0-17 Effectiveness of gadolinium bed is presented as a function of frequency and displaced fluid volume, (a) cold blow, (b) hot blow.

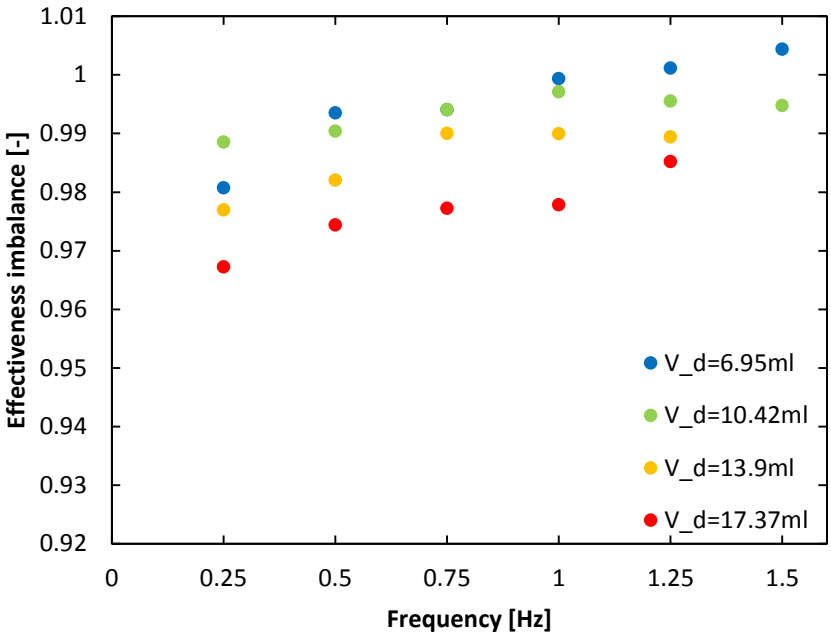

Figure 0-18 Effectiveness imbalance between hot blow and cold blow for gadolinium bed is presented as a function of frequency and displaced fluid volume.

The effectiveness for gadolinium bed and the effective imbalance are shown in Figure 4-17 and 4-18. The cold blow effectiveness is more sensitive to the utilization values, due to the lower value of specific heat capacity of gadolinium at higher temperatures. This causes an increase of the local utilization near the hot end, leading to a significant source-temperature penetration through the bed after the cold blow and a severe effectiveness imbalance as well, as displayed in Figure 4-18.

The results of tests using gadolinium bed with extended dead volumes are shown below.

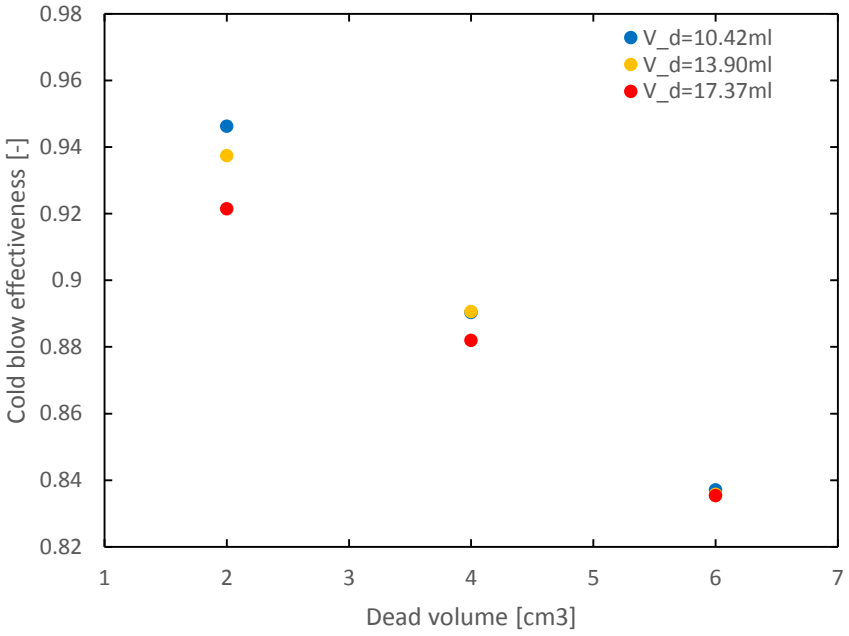

(a)

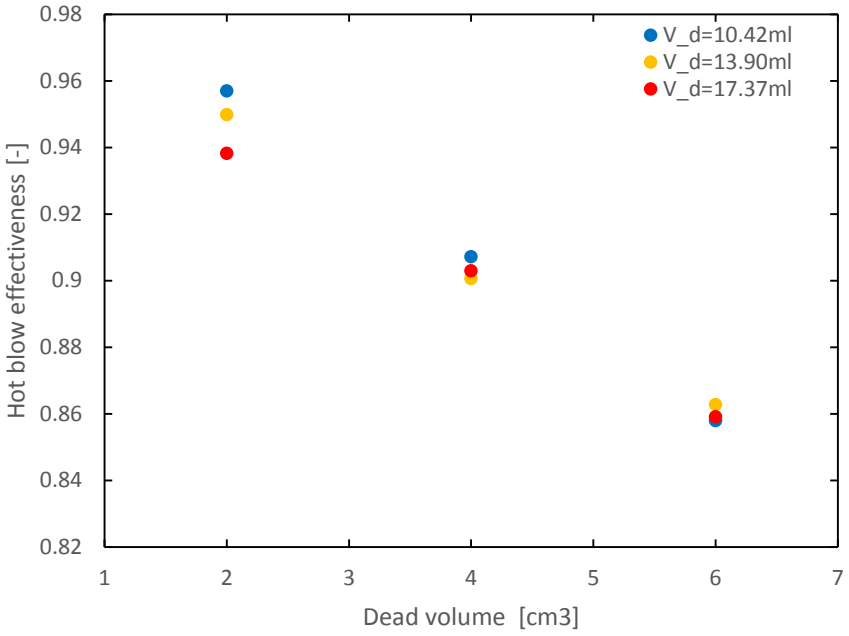

(b)

Figure 0-19 Effectiveness of gadolinium bed is presented as a function of dead volume size and displaced fluid volume , (a) cold blow, (b) hot blow.

Based on the effectiveness figures and the inlet temperature profile figures of gadolinium spheres bed, we can see that the effectiveness decreases with increasing

dead volume extension, and the effectiveness of the cold blow is always lower than that of the hot blow.

This chapter has summarized the experimental data. In the next chapter simulations of the experiments are carried out and results are compared to experimental data.

Simulation Results

This chapter shows the results of the numerical modeling, and compares simulated results with the experimental results.

5.1 Pressure Drop

Making use of Equation 3.5 to build the numerical model for pressure drop and prescribing all experimental parameters leads to a representative simulation result as below, showing the transient pressure drop through the regenerator bed. The waveform generated by the simulation is symmetric in time due to the assumption of sinusoidal velocity. The phase discrepancy between the peaks of the simulation and those of the experimental data can be caused by the non-sinusoidal flow velocity resulting from the crank mechanism of the experimental setup.

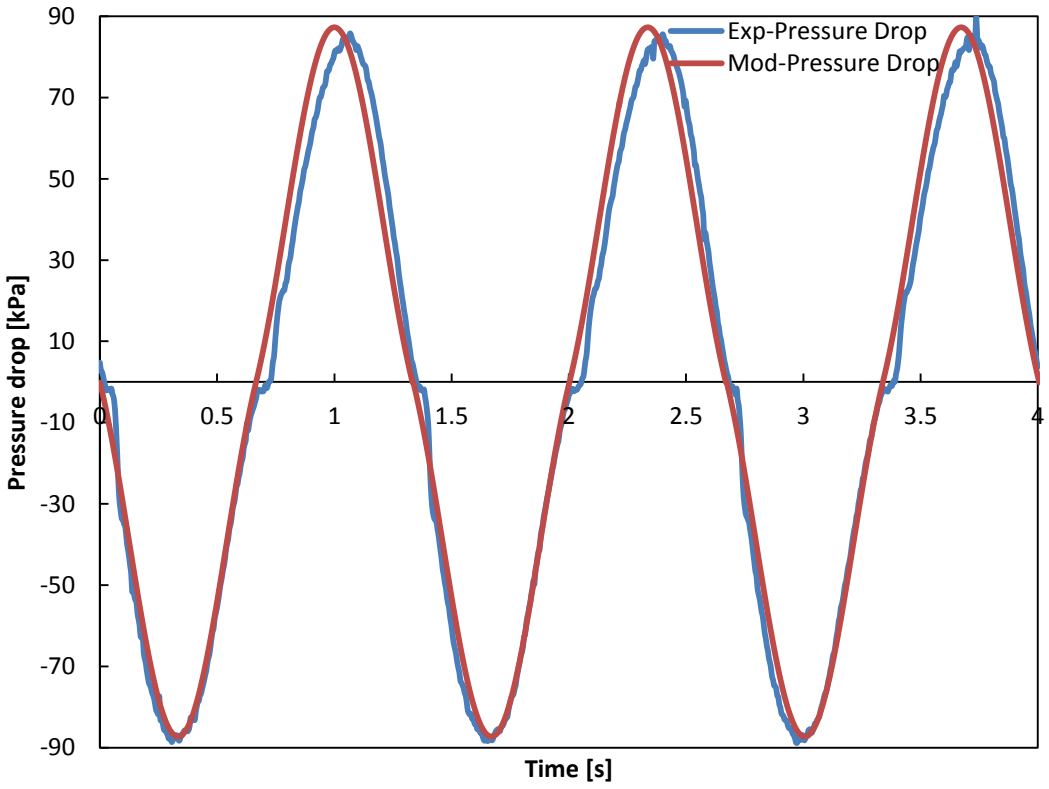

Figure 0-1 The pressure drop simulation is compared with experimental data, using gadolinium bed with displaced fluid volume of 13.9 cm^3 and operating frequency of 0.75 Hz.

Based on the transient pressure drop simulation, the average pressure drops for various operating conditions are calculated and shown in Figures 5-2 through 5-4..

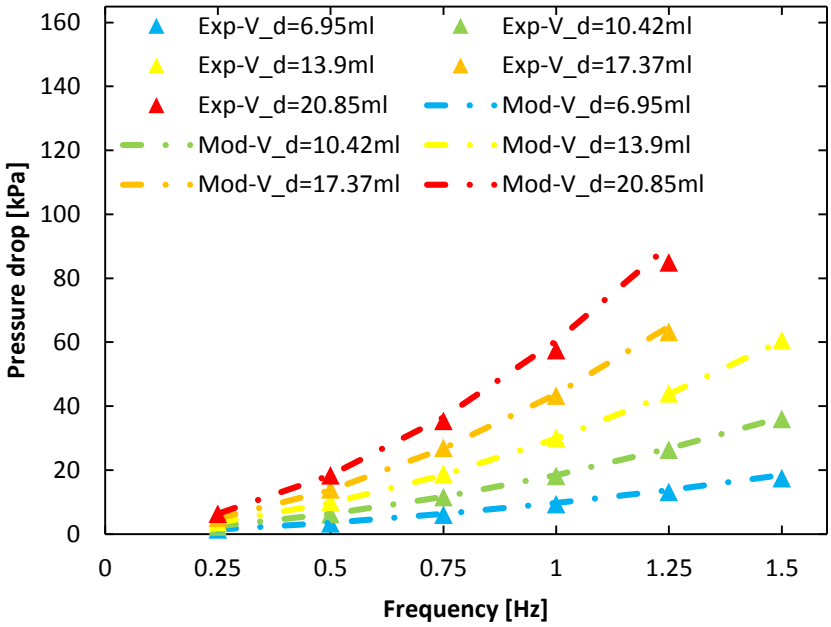

Figure 0-2 Model-predicted average pressure drop for stainless steel bed is compared with experimental data, as a function of frequency and displaced fluid volume.

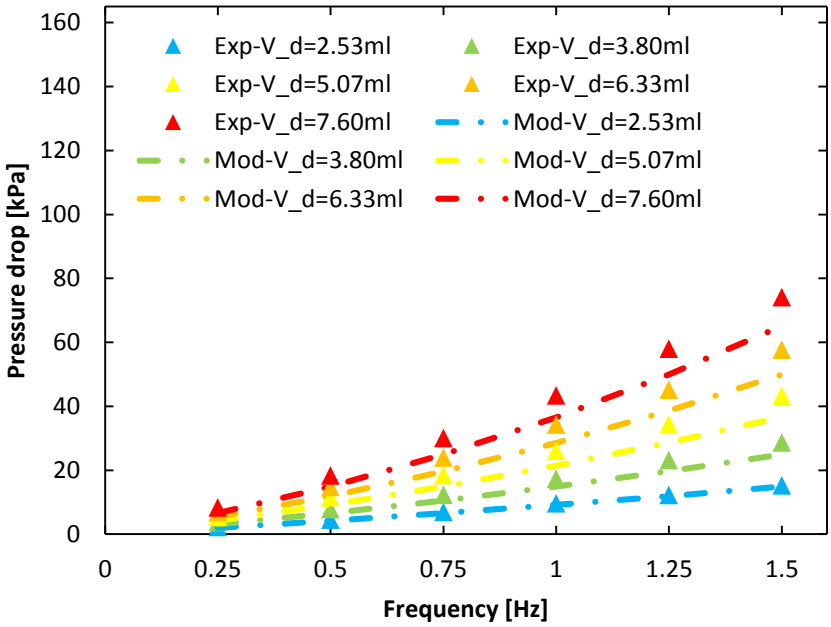

Figure 0-3 Model-predicted average pressure drop for lead bed is compared with experimental data, as a function of frequency and displaced fluid volume

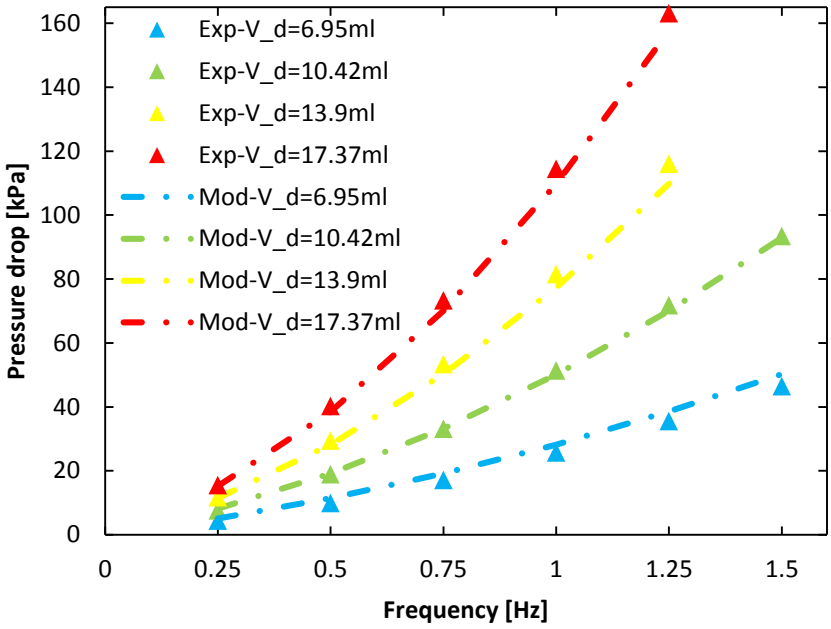

Figure 0-4 Model-predicted average pressure drop for gadolinium bed is compared with experimental data, as a function of frequency and displaced fluid volume

In general, the simulated pressure drop closely matches the measured values and the sensitivity to frequency for all data points. The general trends will be discussed further in Chapter 6.

5.2 Energy Balance

The simulation results presented in this section do not include the dead volume effect, further comparison with simulation containing dead volume effect is done in Chapter 6.

5.2.1 Transient Temperature Field

A transient heat and mass transfer model is created using Equation 3.48 and 3.49. The commercial software COMSOL Multiphysics is used to solve the coupled partial differential equations. The solution is carried out through a number of cycles until cyclic steady state is approached. Cyclic-steady state is determined by setting the tolerance on temperature change between complete cycles at any location to be less than 0.005 K.

Figure 5-5 to 5-7 show the transient fluid temperature fields determined by the model, using the average of solid and fluid temperatures, with comparison to the experimental data, for stainless steel, lead and gadolinium regenerator beds.

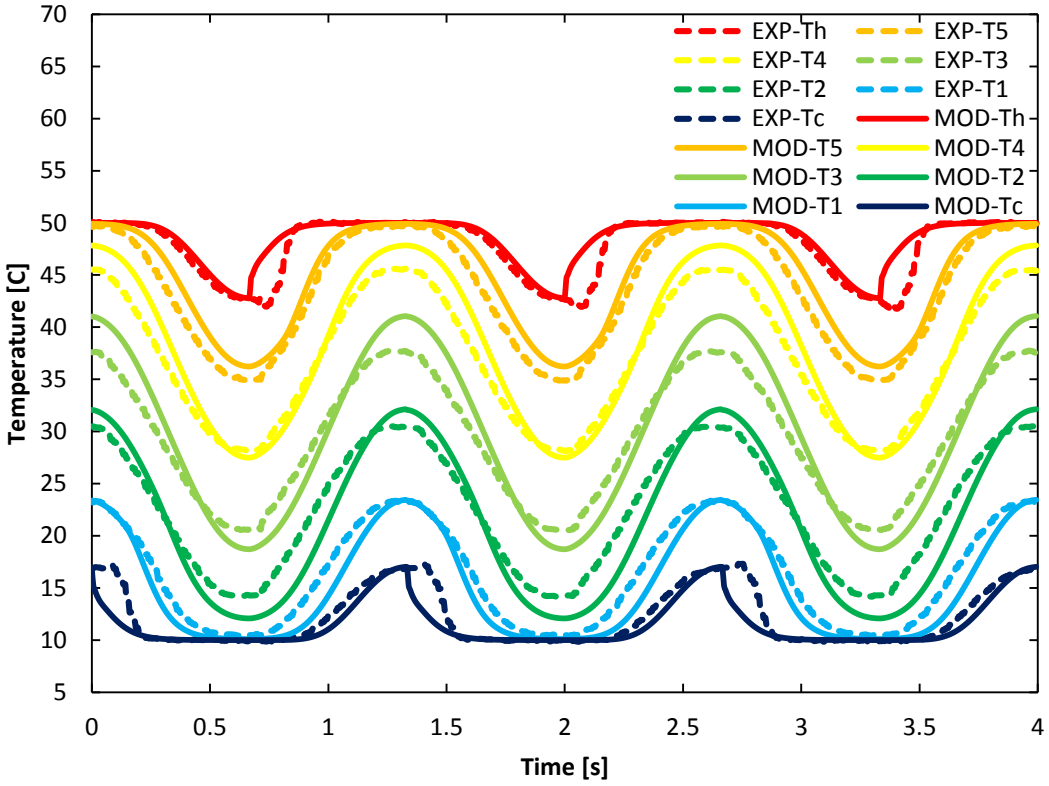

Figure 0-5 Model-predicted temperature variation taking average values between solid and fluid for stainless steel bed is compared with experimental data, under displaced volume of 13.9 cm^3 and operating frequency of 0.75 Hz.

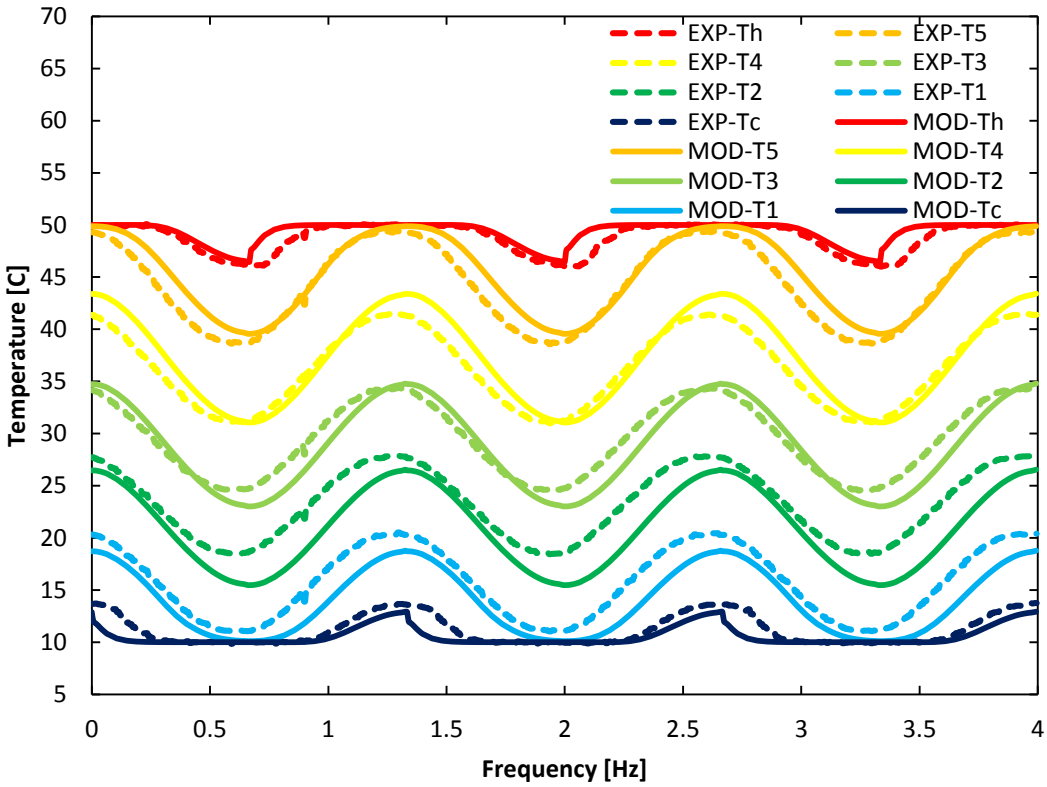

Figure 0-6 Model-predicted temperature variation taking average values between solid and fluid for lead bed is compared with experimental data, under displaced volume of 5.07 cm^3 and operating frequency of 0.75 Hz.

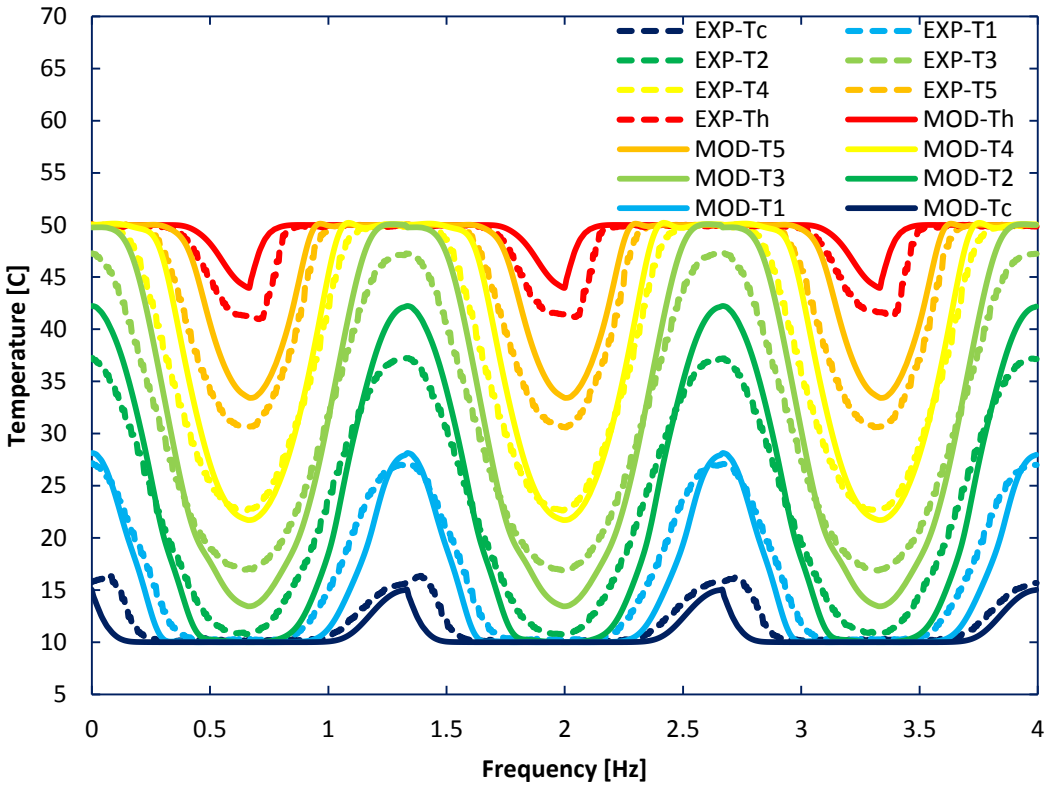

Figure 0-7 Model-predicted temperature variation taking average values between solid and fluid for gadolinium bed is compared with experimental data, under displaced volume of 13.9 cm^3 and operating frequency of 0.75 Hz.

As can be seen in the plots above, the simulation data generally follows the dynamic response of the measured temperatures. It should be noted that the thermocouple tips are embedded in the regenerator matrix, the tip will be in contact with both fluid and solid. Thus, the measured data may represent some average of the local fluid and solid temperatures.

5.2.2 Regenerator Effectiveness

Using Equation 2.11 and 2.12, effectiveness is determined based on the simulated average temperatures of solid and fluid at each end of the regenerator. Simulation results are compared to the experimental results presented in Chapter 4.

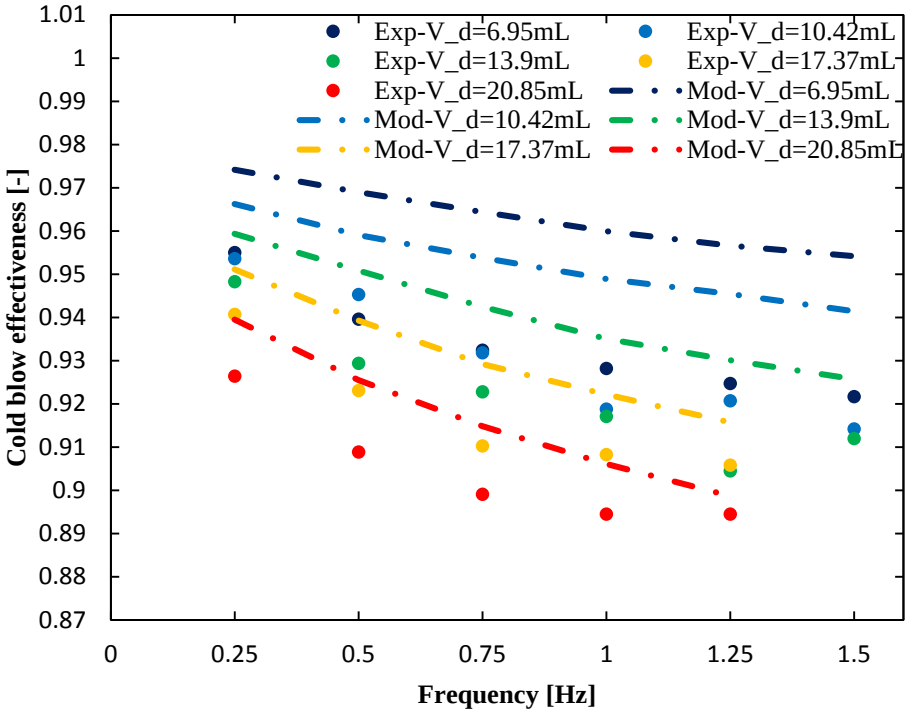

(a)

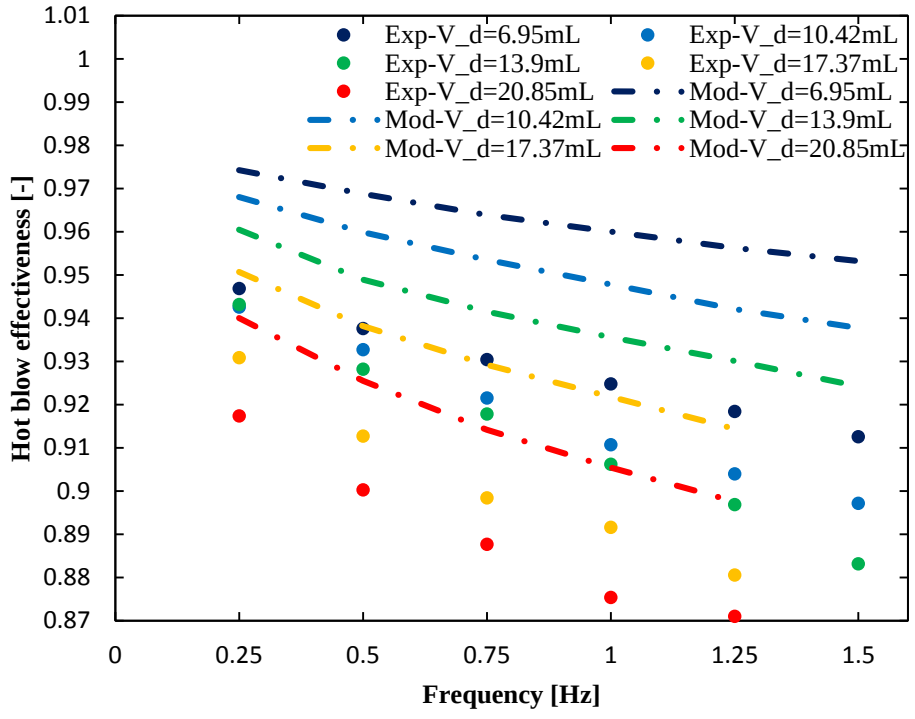

\

(b)

Figure 0-8 Model-predicted effectiveness for stainless steel bed is compared with experimental data, as function of displaced fluid volume and frequency, (a) cold blow, (b) hot blow.

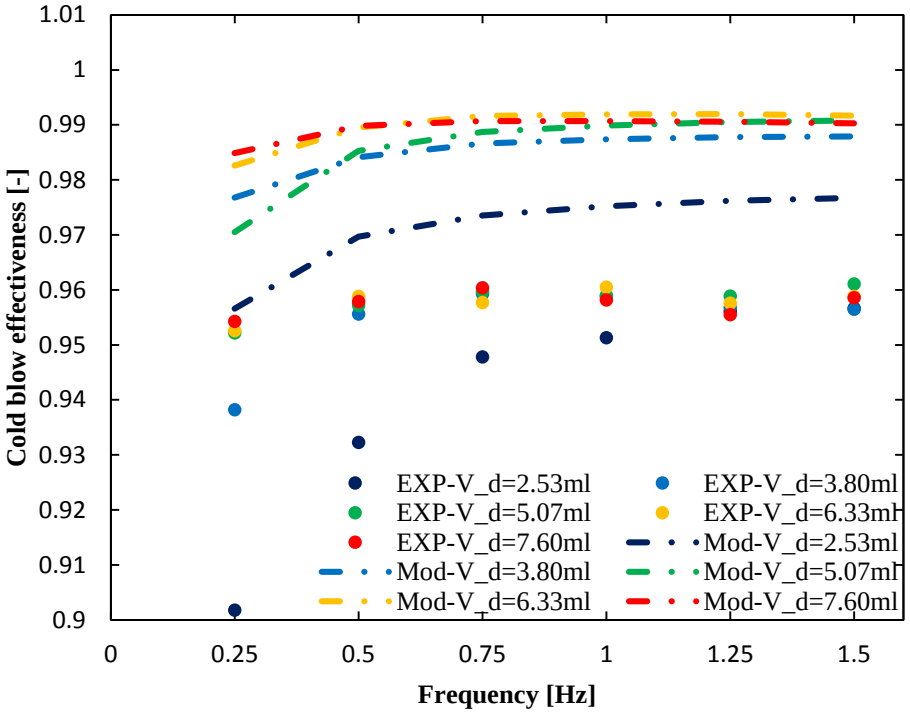

(a)

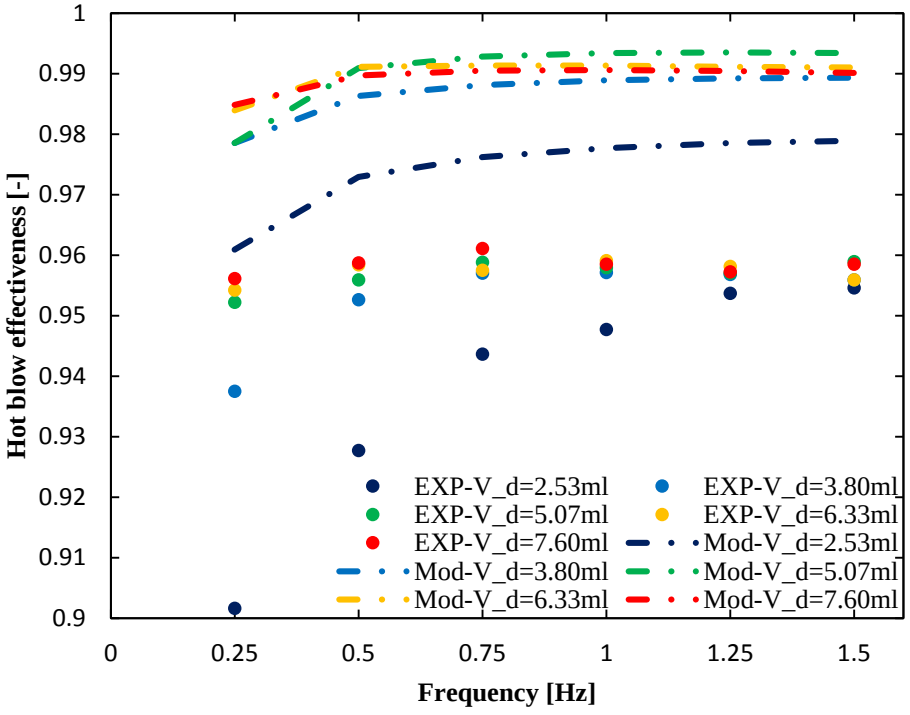

(b)

Figure 0-9 S Model-predicted effectiveness for lead bed is compared with experimental data, as function of displaced fluid volume and frequency, (a) cold blow, (b) hot blow.

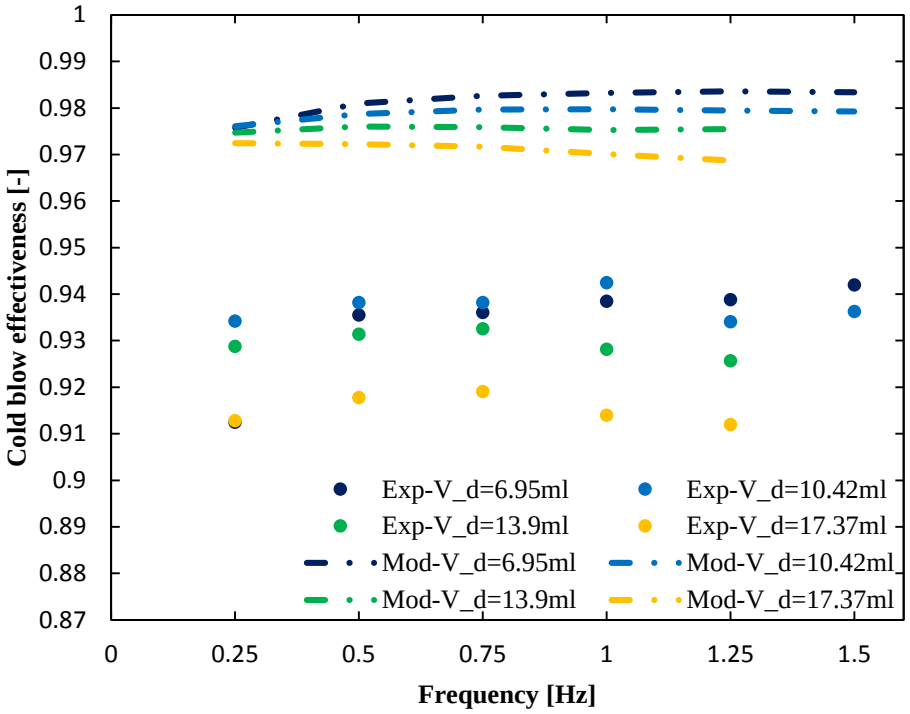

(a)

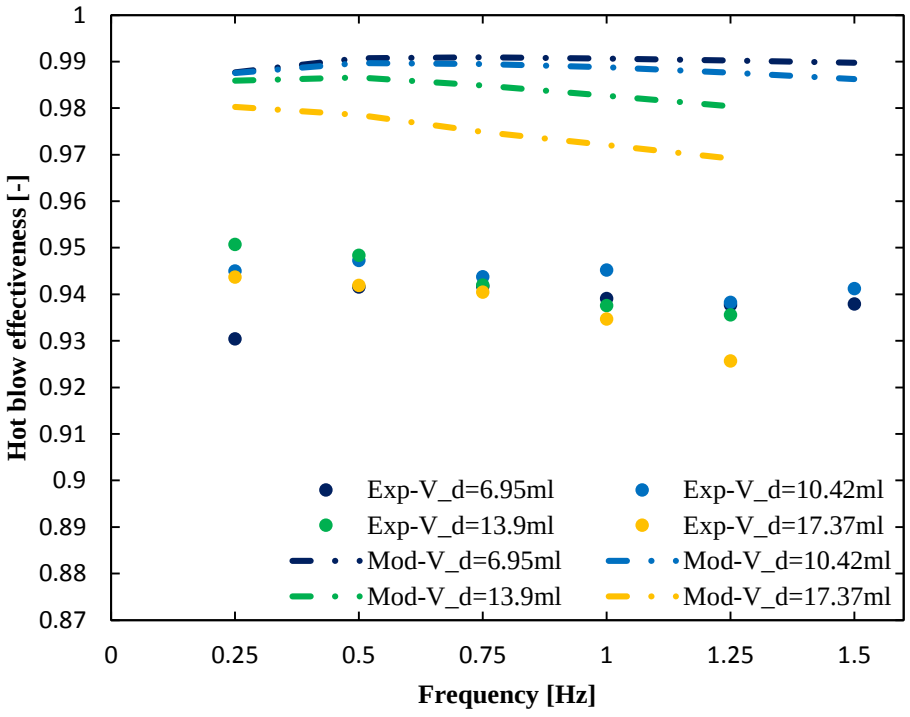

(b)

Figure 0-10 Model-predicted effectiveness for gadolinium bed is compared with experimental data, as function of displaced fluid volume and frequency, (a) cold blow, (b) hot blow.

Table 0-1 Maximum and average percentage difference between simulation and experimental data

	Stainless steel bed		Lead bed		Gadolinium bed	
	Cold blow	Hot blow	Cold blow	Hot blow	Cold blow	Hot blow
Maximum [%]	3.5	4.6	6.1	6.6	6.9	5.1
Average [%]	2.1	3.3	3.2	3.5	6.2	4.7

As can be seen in Figures 5-8 through 5-10 and Table 5-1, the simulated results tend to over predict the measured data; however, sensitivity to displaced fluid volume and frequency tend to agree. The simulation for stainless steel spheres bed presents the least deviation against the experimental results among the three types of regenerator beds.

Further analysis of the experimental and simulation results will be discussed in the next chapter. A sensitivity analysis will be performed using the numerical model to clarify how the simulated physical mechanisms impact regenerator behavior.

Discussion

In this chapter, the results of the experiments and simulation are analyzed to determine possible causes for observed difference. The impacts of uncertainties in geometric and property data are examined.

6.1 Friction Factor

According to Ergun's study [32], the pressure drop through regenerator bed can be calculated below.

$$\frac{\overline{\Delta p}}{L_{reg}} = \frac{1-e}{e^3}\frac{\rho_f \bar{u}_D^2}{D_s}[150\frac{\mu(1-e)}{\rho u_D D_s}+1.75] \tag{6.1}$$

Two parameters are defined here: f' is friction factor and R_e' is Reynolds number for porous medium.

$$f' = \frac{\Delta p}{L_{reg}}\frac{D_s}{\rho_f \bar{u}_D^2}(\frac{e^3}{1-e}) \tag{6.2}$$

$$R_e' = \frac{\rho \bar{u}_D D_s}{\mu(1-e)} \tag{6.3}$$

Substituting both parameters into Equation 6.1 gives get an expression as follows.

$$f' = \frac{150}{R_e'}+1.75 \tag{6.4}$$

where the first term on the right hand side is Kozeny-Carman factor and the second term is Burke-Plummer factor. The influence of Reynolds number on each term in Equation 6.4 is demonstrated in Figure 6-1. As we can see, the friction factor drops with Reynolds number and approaches the value of 1.75.

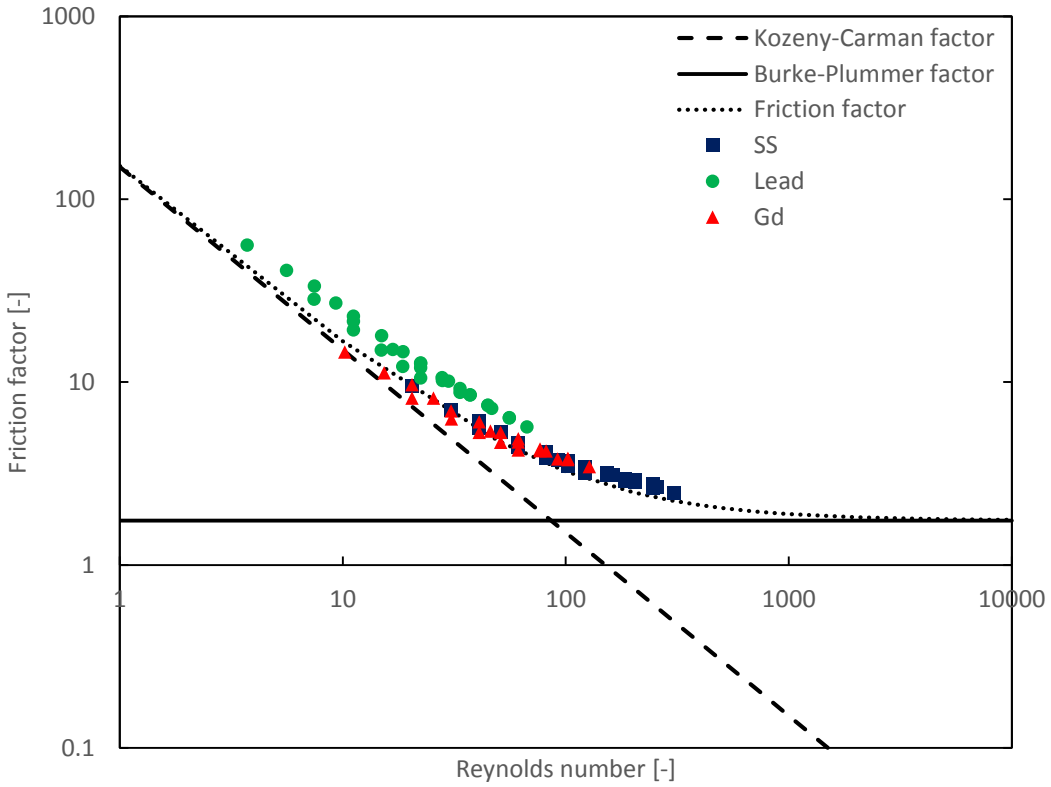

Figure 0-1 Friction factors generated by experimental pressure drop data are compared with friction factors calculated using various Reynolds numbers.

As shown in Figure 6.1, the friction factors calculated based on experimental pressure drop data using Equation 6.2 are plotted, and match up with the predicted values generated by Equation 6.4 with varying Reynolds number. Average pressure drop increases with superficial velocity; on the other hand, combining Equation 6.3 and 6.4, friction factor decreases with superficial velocity. The relationship between average pressure drop and friction factor is not linear. As far as a single type of regenerator bed is concerned, tests subjected to higher superficial velocities usually present higher average pressure drop and lower friction factors.

6.2 Regenerator Effectiveness Analysis

In this section, some possibilities are studied to explain the discrepancies between simulation and experimental data.

6.2.1 Viscous Dissipation

Viscous dissipation occurs when the fluid travels through the regenerator bed, and this amount of energy affects the energy transfer in the system. Viscous dissipation is neglected when determining the regenerator effectiveness experimentally, as it has a negligible impact. To validate this assumption, the effectiveness taking the viscous term into consideration is calculated, as shown in Equation 2.8 and 2.10, and compared them with the ones determined by Equation 2.11 and 2.12.

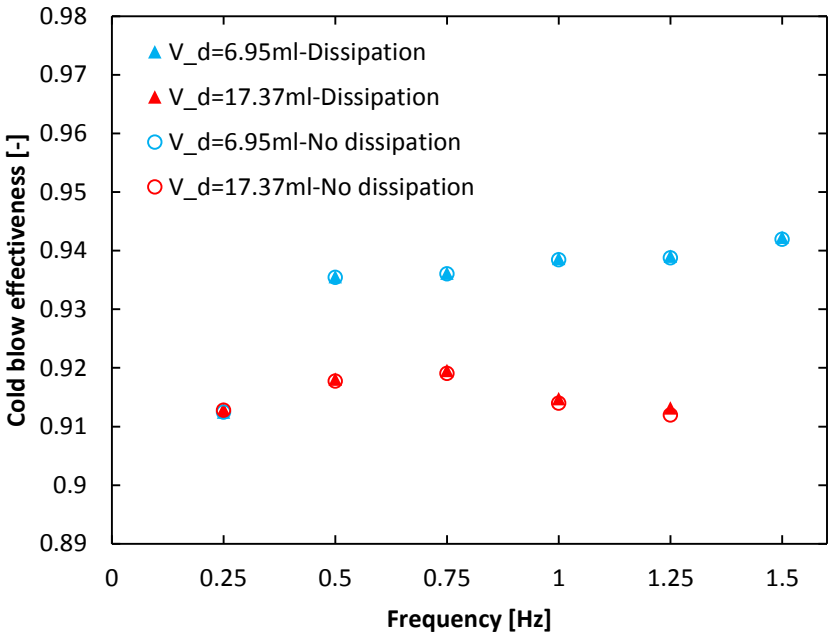

(a)

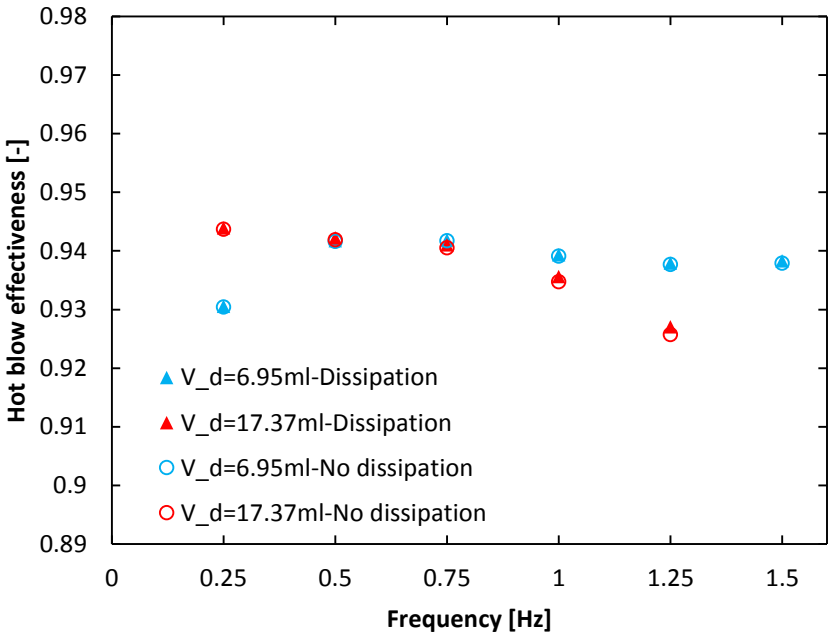

(b)

Figure 0-2 Effectiveness including and not including viscous dissipation are compared with each other, as a function of displaced fluid volume and frequency, (a) cold blow, (b) hot blow.

As shown in the figures above, the viscous dissipation gives negligible influence to the regenerator effectiveness calculation. Those two types of effectiveness

calculations are nearly overlapping each other, and the relatively distinguishable difference only takes place when both the operating frequency and the displaced volume get big enough. This point is validated by our numerical model as well.

6.2.2 Heat Convection Coefficient Study

To investigate the sensitivity of the model on the heat convection term, we assume a hypothetical scaling factor, in front of the convection terms in Equation 3.46 and 3.47. The impacts of changing the base value by 0.5 and 1.5 are shown in Figure 6-3.

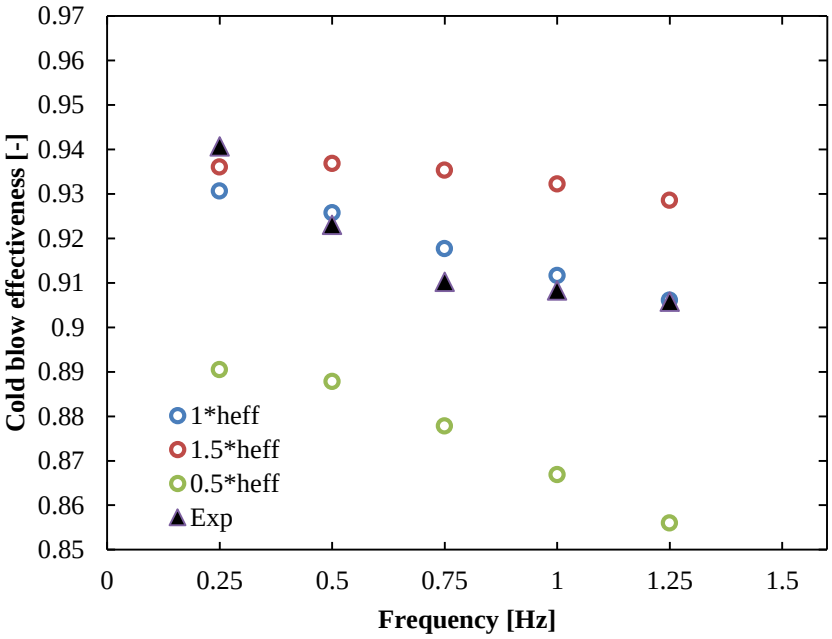

(a)

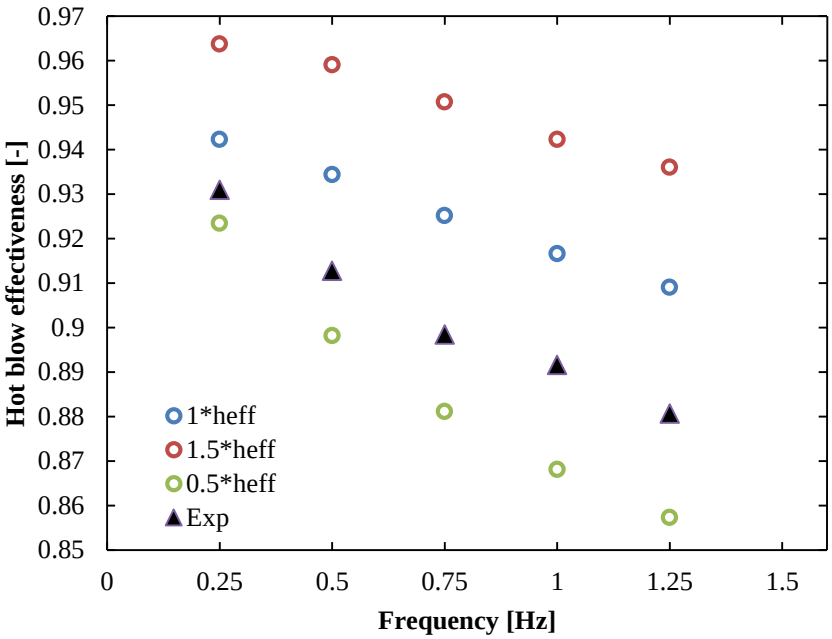

(b)

Figure 0-3 Various values of convection coefficient are used to calculated the regenerator effectiveness for stainless steel bed, under displaced fluid volume of 17.37 ml, (a) cold blow, (b) hot blow.

According to the simulation results, enhanced convection between the solid matrix and the fluid improves the regenerator performance. A reduction in convection

coefficient tends to correct the hot blow simulations to match the experiments, but reduces the match for the cold blow.

6.2.3 Dispersion Study

Similarly, we assume another two scaling factors for the dynamic and static conduction terms in Equation 3.46 and 3.47, respectively.

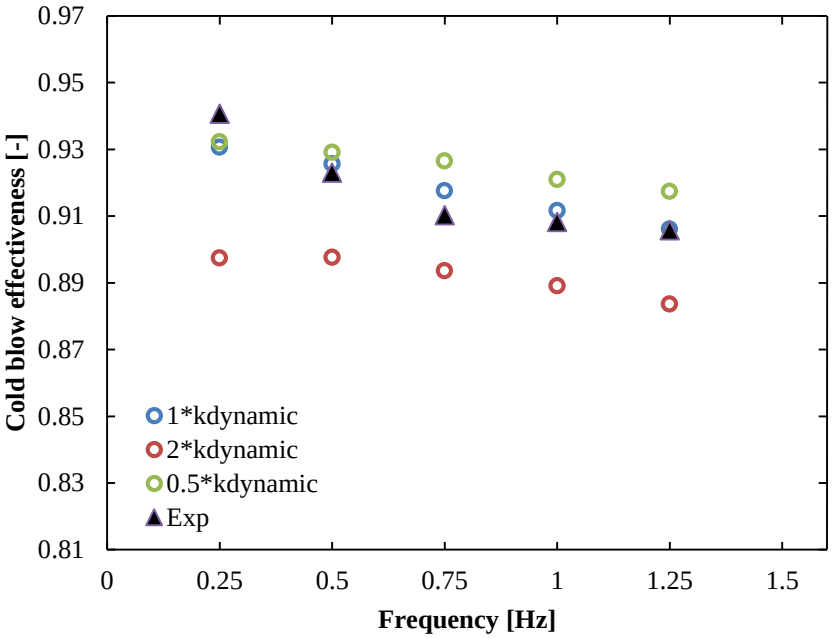

(a)

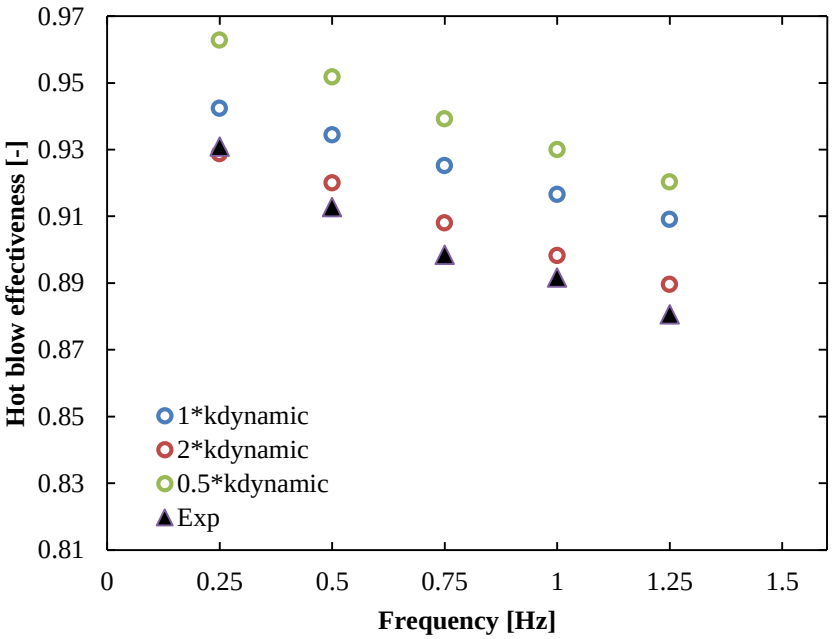

(b)

Figure 0-4 Various values of dynamic conductivity are used to calculated the regenerator effectiveness for stainless steel bed, under displaced fluid volume of 17.37 ml, (a) cold blow, (b) hot blow.

Increasing the dynamic conduction decreases the performance of the regenerator, maintaining almost same effect through the studied frequency range. Similar phenomena are also observed in the models based on lead and gadolinium beds.

6.2.4 Static Conductivity Study

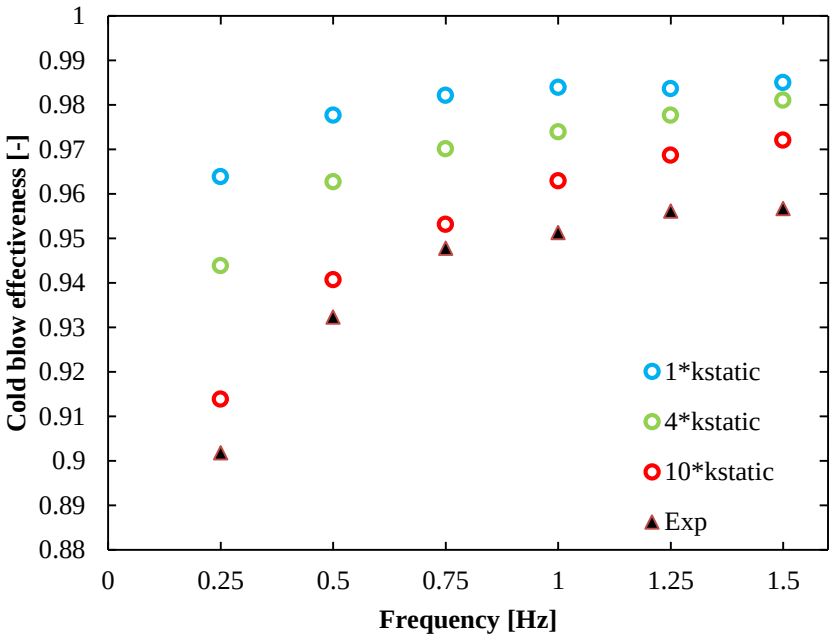

(a)

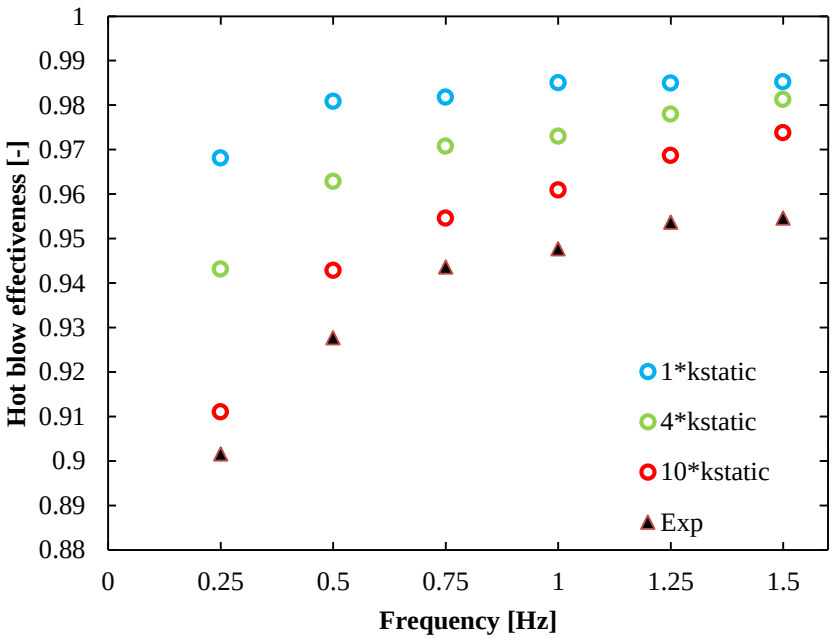

(b)

Figure 0-5 Various values of static conductivity are used to calculated the regenerator effectiveness for lead bed, under displaced fluid volume of 2.53 ml, (a) cold blow, (b) hot blow.

As shown in the figure above, the scaling factor for k_{static} has more impact on the low-frequency scenarios than the high-frequency ones. It means that if we add same amount of static conduction to the regenerator, the regenerator performance will be

reduced especially when the flow rate is low. An order of magnitude increase in the static conductivity appears to correct the simulation results so that both cold and hot blows align with the experimental results for lead bed. While an order of magnitude increase is difficult to imagine, one possible way for a high static conductivity is because of larger contact areas between particles. Normally, for spherical particles, a point contact is assumed; however, lead is a soft ductile material that can easily deform. Deformation during packing may increase contact areas and effective thermal conductivity.

6.3 Ratio of Dead Volume and its impact

In AMR cycles the best performance arises when the utilization is on the order of 1, and typical values are in the range of 0.5-1. For AMRs using water, utilization are roughly equal to the displaced volume of water divided by the volume of solid material. In Figure 6-6, the impact of dead volume on effectiveness is plotted where the dead volume is normalized by the displaced volume.

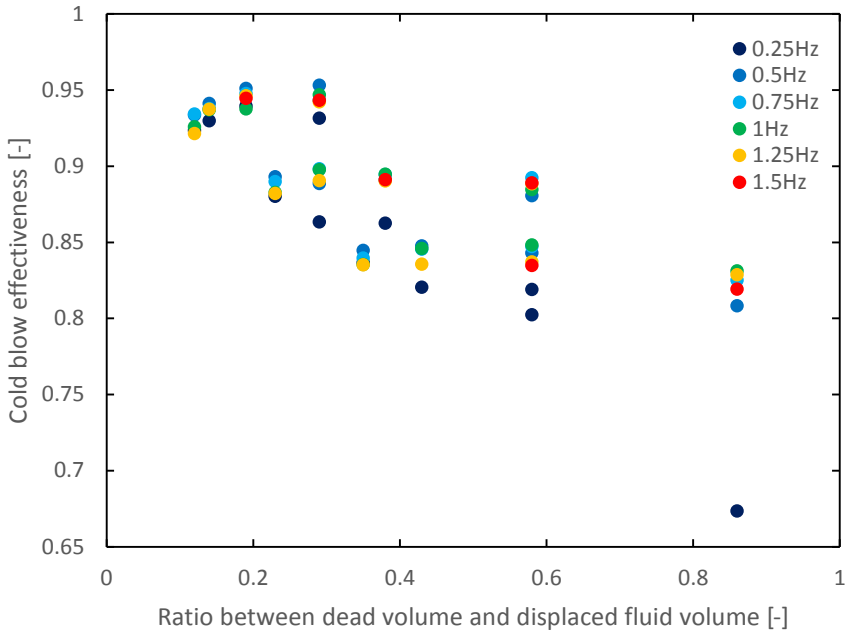

(a)

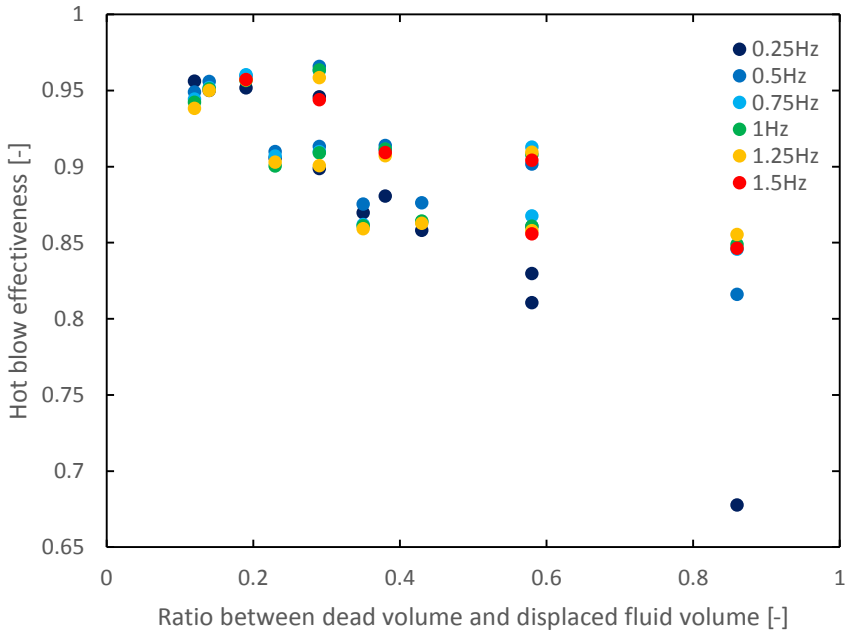

(b)

Figure 0-6 Experimental data of regenerator effectiveness is presented as a function of operating frequency and ratio between dead volume and displaced fluid volume, using gadolinium bed, (a) cold blow, (b) hot blow.

As shown in Figure 6-7 (a) and (b), the scattered regenerator effectiveness with various operating frequencies and utilizations tend to decrease as the dead volume increases. As the dead volume increase to 0.8, the regenerator performance is reduced significantly. This finding agrees with a recent study on an AMR where dead volume effects are considered [19].

6.4 Dead Volume Correction in Simulation

In an ideal case, the inlet temperature is always same as the source temperature during a single blow. While, in reality, due to the dead volumes existing between the regenerator and the heat exchanger, there is a transition period when the inlet fluid temperature changes from the regenerator temperature to the source temperature after the flow direction is reversed.

To investigate the dead volume effect, we take the parasitic dead volume in the experimental device into consideration, which is 2 cm^3 on each end of the regenerator. Simulations containing dead volume effect give new effectiveness as shown in Figure 6-7.

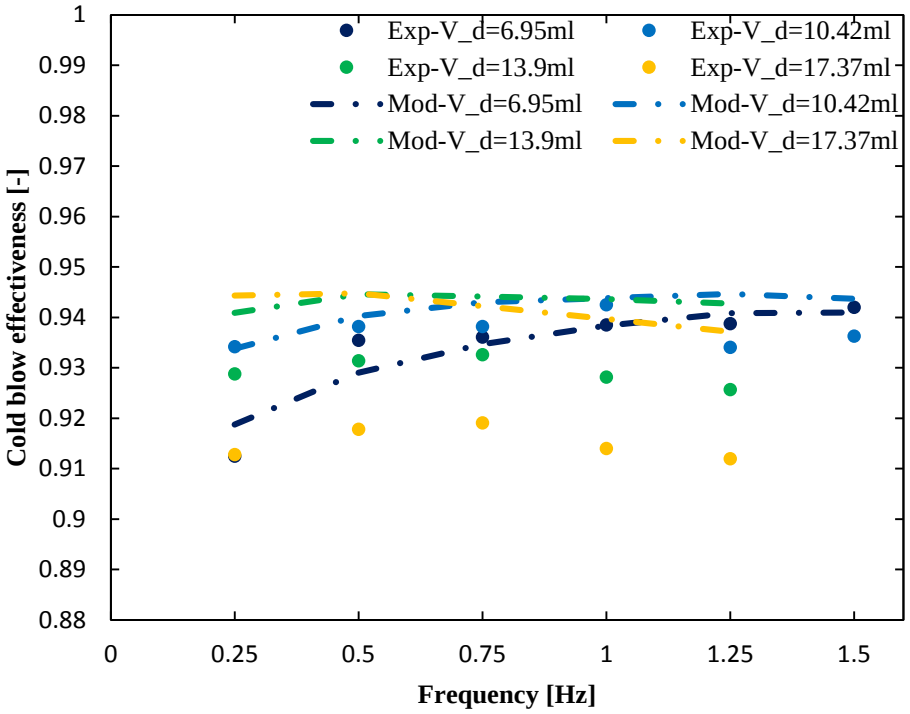

(a)

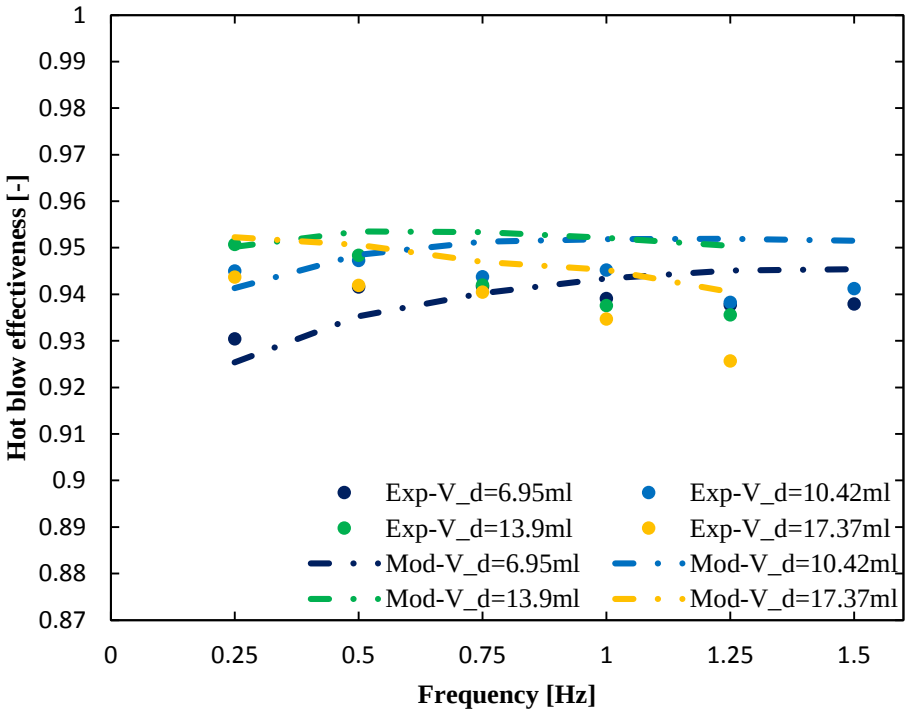

(b)

Figure 0-7 Model-predicted regenerator effectiveness for gadolinium bed is compared with experimental data, with dead volume effect included in the model, as function of operating frequency and displaced fluid volume, (a) cold blow, (b) hot blow.

Basically, the dead volume effect reduces the regenerator effectiveness comparing Figure 6-9 with Figure 5-10, and corrects the trends in some degree, driving the simulation to approach the experimental data. The average percentage difference between simulation and experimental data is reduced to 1 percent.

This chapter provides a closer analysis of the experimental data and simulation results. Sensitivity studies are carried out on important experimental parameters including viscous dissipation, heat convection coefficient, effective dynamic conductivity, effective static conductivity and dead volume either experimentally or numerically. Among the parameters under investigation, dead volume presents a significant impact on the regenerator effectiveness and tends to drive the simulation to approach the experimental results. The value of dead volume normalized by the displaced fluid volume is emphasized, as theoretically regenerator performance is decreased when higher proportion of displaced volume is trapped in dead volume. Statistically, the regenerator effectiveness goes below 90%, which is a big energy loss, when the dead volume reaches 80% of the displaced volume. Based on the dead volume study on passive regeneration, we can confirm the adverse impact of dead volume on AMR devices and suggest the introduction of dead volume in AMR models to account for the parasitic dead volume effect in the devices. At the same time, the constraint of the current one-dimensional model is realized, and phenomena in experiments including transverse conduction and flow heterogeneity call for implementation of two-dimensional model. The next chapter will make conclusions to the testing apparatus and the passive regenerator model.

Conclusions and Recommendations

This thesis introduced an experimental method to test the hydraulic and thermodynamic properties of passive regenerators. Important information including the pressure drop and axial temperature gradient were extracted from various regenerator beds. And the regenerator thermodynamic performances were evaluated via the calculation of regenerator effectiveness. Based on the current experimental device, a transient numerical model was built, which could give good predictions of the regenerator performances.

In the experimental part, three kinds of passive regenerator beds were tested subjected to sinusoidal oscillating flow. Based on the calculated regenerator effectiveness, we can see that the performance of stainless steel bed could be well explained by the NTU variation. The lead bed brought questions as it demonstrated opposite trends compared with the stainless steel bed. And the gadolinium bed showed as a combination of the stainless steel bed and the lead bed, with respect to various utilizations. The temperature dependence of specific heat capacity of the material generates imbalance between hot and cold blow effectiveness. In the case that the temperature dependence of specific heat capacity is negligible, like stainless steel and lead, the two types of effectiveness share similar values and sensitivity with each other. While, for materials like gadolinium which specific heat capacity has a significant temperature dependence, the difference between hot and cold blow effectiveness becomes considerable. For regenerators used in magnetic refrigeration, the hot blow effectiveness counts more as refrigeration is generated on the cold side and a fixed hot side temperature is assumed.

Among the three types of regenerator beds, the simulations of stainless steel showed the best agreement with the experimental data. A sensitivity study showed that increased static conductivity could lead to a good agreement between simulations and experiments for the lead regenerator. Dead volume, as a key point in this work, affects

passive regenerator performance significantly especially when the size of dead volume approaches that of the displaced fluid volume, and also changes the dependence of regenerator effectiveness on utilization and frequency.

There are a number of areas for future investigation relating to the theoretical and experimental methods.

Good determination of the flow reversing point between blows helps to assess the regenerator effectiveness precisely. To make the numerical model generate better predictions of the regenerator performance, the dead volume should be determined accurately, and more sensitivity studies are needed to quantify its impact on the regenerator effectiveness. There is evidence indicating a transverse temperature gradient in the regenerator bed, and further numerical analysis can help to identify its role in the determination of the regenerator performance. An estimation of heat loss in the junctions between the heat exchangers and the regenerator may help explain some of the unusual tendencies of the regenerator effectiveness with respect to increasing frequency. In addition, consistent and modular thermal insulation for the device is required for the repeatability of the experiments.

Simulation tool can always be modified to eliminate the discrepancy with the experiments as much as possible, like the sensitivity analysis we conduct in chapter 6, and that is one of the vital advantages that numerical models possess. This correcting process helps explain the phenomena we observe in the tests. Possible corrections should be validated by various experimental results, and exaggerating or reducing one single factor excessively without any foundation should be avoided.

Reference

[1] J. Conti, “Annual Energy Outlook 2014 with Projections to 2040,” *U.S. Energy Inf. Adm.*, 2014.

[2] T. J. Wallington, M. P. Sulbaek Andersen, and O. J. Nielsen, “Atmospheric chemistry of short-chain haloolefins: Photochemical ozone creation potentials (POCPs), global warming potentials (GWPs), and ozone depletion potentials (ODPs),” *Chemosphere*, vol. 129, pp. 135–141, 2014.

[3] V. K. Pecharsky and K. A. Gschneidner Jr., “Magnetocaloric Effect,” *Encycl. Condens. Matter Phys.*, pp. 236–244, 2005.

[4] K. a G. Jr. and V. K. Pecharsky, “The influence of magnetic field on the thermal properties of solids,” *Mater. Sci. Eng. A*, vol. 287, no. 2, pp. 301–310, 2000.

[5] V. K. Pecharsky and K. a Gschneidner Jr, “Magnetocaloric effect and magnetic refrigeration,” *J. Magn. Magn. Mater.*, vol. 200, no. January, pp. 44–56, 1999.

[6] V. K. Pecharsky and K. a. Gschneidner, “Advanced magnetocaloric materials: What does the future hold?,” *Int. J. Refrig.*, vol. 29, no. 8, pp. 1239–1249, 2006.

[7] E. Brück, O. Tegus, D. T. Cam Thanh, N. T. Trung, and K. H. J. Buschow, “A review on Mn based materials for magnetic refrigeration: Structure and properties,” *Int. J. Refrig.*, vol. 31, no. 5, pp. 763–770, 2008.

[8] A. Smith, C. R. H. Bahl, R. Bjork, K. Engelbrecht, K. K. Nielsen, and N. Pryds, “Materials challenges for high performance magnetocaloric refrigeration devices,” *Adv. Energy Mater.*, vol. 2, no. 11, pp. 1288–1318, 2012.

[9] R. Bjørk, C. R. H. Bahl, a. Smith, and N. Pryds, “Review and comparison of magnet designs for magnetic refrigeration,” *Int. J. Refrig.*, vol. 33, no. 3, pp. 437–448, 2010.

[10] R. Bjørk and K. Engelbrecht, “The influence of the magnetic field on the performance of an active magnetic regenerator (AMR),” *Int. J. Refrig.*, vol. 34, no. 1, pp. 192–203, 2011.

[11] J. A. Barclay and S. Sarangi, “Selection of Regenerator Geometry for Magnetic Refrigerator Applications.” 1984.

[12] K. Engelbrecht, D. Eriksen, C. R. H. Bahl, R. Bjørk, J. Geyti, J. a. Lozano, K. K. Nielsen, F. Saxild, a. Smith, and N. Pryds, “Experimental results for a novel rotary active magnetic regenerator,” *Int. J. Refrig.*, vol. 35, no. 6, pp. 1498–1505, 2012.

[13] P. V. Trevizoli and J. R. Barbosa, “Entropy Generation Minimization analysis of oscillating-flow regenerators,” *Int. J. Heat Mass Transf.*, vol. 87, pp. 347–358, 2015.

[14] a. Tura and a. Rowe, “Permanent magnet magnetic refrigerator design and experimental characterization,” *Int. J. Refrig.*, vol. 34, no. 3, pp. 628–639, 2011.

[15] a. Tura, K. K. Nielsen, and a. Rowe, “Experimental and modeling results of a parallel plate-based active magnetic regenerator,” *Int. J. Refrig.*, vol. 35, no. 6, pp. 1518–1527, 2012.

[16] P. Trevizoli, Y. Liu, A. Tura, A. Rowe, and J. Barbosa, “Experimental assessment of the thermal–hydraulic performance of packed-sphere oscillating-flow regenerators using water,” *Exp. Therm. Fluid Sci.*, vol. 57, pp. 324–334, Sep. 2014.

[17] *Advances in Cryogenic Engineering: Parts A & B*. Springer Science & Business Media, 2012.

[18] A. Kitanovski, J. Tušek, U. Tomc, U. Plaznik, M. Ozbolt, and A. Poredoš, *Magnetocaloric Energy Conversion: From Theory to Applications*. Springer, 2014.

[19] I. Park, Y. Kim, and S. Jeong, “Development of the tandem reciprocating magnetic regenerative refrigerator and numerical simulation for the dead volume effect,” *Int. J. Refrig.*, vol. 36, no. 6, pp. 1741–1749, 2013.

[20] K. K. Nielsen, J. Tusek, K. Engelbrecht, S. Schopfer, a. Kitanovski, C. R. H. Bahl, a. Smith, N. Pryds, and a. Poredos, “Review on numerical modeling of active magnetic regenerators for room temperature applications,” *Int. J. Refrig.*, vol. 34, no. 3, pp. 603–616, 2011.

[21] B. Yu, M. Liu, P. W. Egolf, and A. Kitanovski, “A review of magnetic refrigerator and heat pump prototypes built before the year 2010,” *Int. J. Refrig.*, vol. 33, no. 6, pp. 1029–1060, 2010.

[22] K. a. Gschneidner and V. K. Pecharsky, “Thirty years of near room temperature magnetic cooling: Where we are today and future prospects,” *Int. J. Refrig.*, vol. 31, no. 6, pp. 945–961, 2008.

[23] Y. Ju and Q. Shen, “Comparative study of oscillating flow characteristics of cryocooler regenerator at low temperatures,” *Front. Energy Power Eng. China*, vol. 3, no. 1, pp. 80–84, 2009.

[24] M. Frischmann, K. Engelbrecht, G. Nellis, and S. Klein, “Heat Transfer Coefficient in a Packed Sphere Regenerator for use in Active Magnetic Regenerative Refrigeration,” *Refrig. Air Cond.*, pp. 1–8, 2008.

[25] “Heat Capacity for Regenerator Material.” [Online]. Available: http://www.cryogenics.nist.gov/MPropsMAY/RegeneratorMaterials/Regenerator Materials rev 09-22-06.htm. [Accessed: 28-Jul-2015].

[26] K. a Gschneidner Jr, “Heat Capacity Measurements of Gadolinium.”

[27] R. Ackermann, *Cryogenic Regenerative Heat Exchangers*. Plenum Press, New York, 1997.

[28] R. K. Shah, *Fundamentals of Heat Exchanger Design*. 2003.

[29] B. S. Baclic, “Misinterpretations of the diabatic regenerator performances,” *J. Heat Mass Transf.*, 1988.

[30] M.Kaviany, *Principles of Heat Transfer in Porous Media*, 2nd ed. Springer.

[31] P. V Trevizoli and J. R. B. Jr, “Modeling of Thermo-Magnetic Phenomena in Active Magnetic Regenerators,” 2013.

[32] S. Ergun, “Fluid flow through packed columns,” *Chem. Eng. Prog.*, vol. 48, no. 2, pp. 89–94, 1952.

[33] G. R. Hadley, “Thermal conductivity of packed metal powders,” *Int. J. Heat Mass Transf.*, vol. 29, no. 6, pp. 909–920, 1986.

[34] N. Wakao and S. Kagei, *Heat and Mass Transfer in Packed Beds*. Taylor & Francis, 1982.

[35] D. A. Nield and A. Bejan, *Convection in Porous Media*, 4th ed. New York City: Springer, 2013.

[36] K. K. Nielsen, G. F. Nellis, and S. a. Klein, "Numerical modeling of the impact of regenerator housing on the determination of Nusselt numbers," *Int. J. Heat Mass Transf.*, vol. 65, pp. 552–560, 2013.

[37] K. L. Engelbrecht, G. F. Nellis, and S. a. Klein, "The Effect of Internal Temperature Gradients on Regenerator Matrix Performance," *J. Heat Transfer*, vol. 128, no. 10, p. 1060, 2006.

[38] F. P. Incropera, D. P. DeWitt, T. L. Bergman, and A. S. Lavine, *Fundamentals of Heat and Mass Transfer*, vol. 6th. 2007.

[39] G. F. Nellis and S. a. Klein, "Regenerative heat exchangers with significant entrained fluid heat capacity," *Int. J. Heat Mass Transf.*, vol. 49, no. 1–2, pp. 329–340, 2006.